HELDA
HELSINGIN YLIOPISTO
HELSINGFORS UNIVERSITET
UNIVERSITY OF HELSINKI

UNIVERSITY OF HELSINKI

https://helda.helsinki.fi

Comparing the Ligand Behavior of N-Heterocyclic Phosphenium and Nitrosyl Units in Iron and Chromium Complexes

Feil, Christoph M.

2019-05-06

Feil , C M , Hettich , T D , Beyer , K , Sondermann , C , Schlindwein , S H , Nieger , M & Gudat , D 2019 , ' Comparing the Ligand Behavior of N-Heterocyclic Phosphenium and Nitrosyl Units in Iron and Chromium Complexes ' , Inorganic Chemistry , vol. 58 , no. 9 , pp. 6517-6528 . https://doi.org/10.1021/acs.inorgchem.9b00737

http://hdl.handle.net/10138/324824
https://doi.org/10.1021/acs.inorgchem.9b00737

unspecified
acceptedVersion

Downloaded from Helda, University of Helsinki institutional repository.

This is an electronic reprint of the original article.

This reprint may differ from the original in pagination and typographic detail.

Please cite the original version.

Comparing the Ligand Behavior of N-Heterocyclic Phosphenium and Nitrosyl Units in Iron and Chromium Complexes

Christoph M. Feil,[a] Thomas D. Hettich,[a] Katharina Beyer,[a] Christina Sondermann,[a] Simon H. Schlindwein,[a] Martin Nieger,[b] and Dietrich Gudat[,a]*

[a] Institute for Inorganic Chemistry, University of Stuttgart, Pfaffenwaldring 55, 70550 Stuttgart, Germany

[b] Department of Chemistry, University of Helsinki P.O. Box 55, 00014 University of Helsinki, Finland

KEYWORDS N-heterocyclic Phosphenium complexes – NO complexes – π-acceptor ligands – electronic structure – ligand centered reactivity

ABSTRACT. N-heterocyclic phosphenium (NHP) and nitrosonium (NO^+) ligands are often viewed as isolobal analogues which share the capability to switch between different charge states and display thus redox 'non-innocent' behavior. We report here on mixed complexes $[(NHP)M(CO)_n(NO)]$ (M = Fe, Cr; n = 2, 3), which permit evaluating the donor/acceptor properties of both types of ligands and their interplay in a single complex. The crystalline target compounds

were obtained from reactions of N-heterocyclic phosphenium triflates with PPN[$Fe(CO)_3(NO)$] or PPN[$Cr(CO)_4(NO)$], respectively, and fully characterized. The structural and spectroscopic (IR, UV-VIS) data support the presence of carbene-analogue NHP ligands with overall positive charge state and π-acceptor character. Even the structural features of the M-NO unit were in all but one product blurred by crystallographic CO/NO disorder, spectroscopic studies and the structural data of the remaining compound suggest that the NO units exhibit nitroxide (NO^-) character. This assignment was validated by computational studies, which reveal also that the electronic structure of iron NHP/NO-complexes is closely akin to that of the Hieber anion, $[Fe(CO)_3(NO)]^-$. The electrophilic character of the NHP units is further reflected in the chemical behavior of the mixed complexes. Cyclic voltammetry and IR-SEC studies revealed that complex [(NHP)$Fe(CO)_2(NO)$] (**4**) undergoes chemically reversible one-electron reduction. Computational studies indicate that the NHP unit in the resulting product carries significant radical character and the reduction may thus be classified as predominantly ligand-centered. Reaction of **4** with sodium azide proceeded likewise under nucleophilic attack at phosphorus and decomplexation, while super hydride and methyl lithium reacted with all chromium and iron complexes via transfer of a hydride or methyl anion to the NHP unit to afford anionic phosphine complexes. Some of these species were isolated after cation exchange, or trapped with electrophiles (H^+, $SnPh_3^+$) to afford neutral complexes representing the products of a formal hydrogenation or hydrostannylation of the original M=P double bond.

Introduction

The application of N-heterocyclic phosphenium ions (NHPs) **I**, **II** (chart 1) as ligands in transition metal complexes has been investigated over several decades.[1-3] The NHPs are commonly

viewed as Lewis-ambiphiles that exhibit both σ-donor and π-acceptor character, and considered as analogues of classic σ-donor/π-acceptor ligands like CO or NO^+.[3] In accord with this perception, the short P–M distance and trigonal planar phosphorus coordination observed for the majority of known phosphenium complexes are rationalized by describing the metal-ligand interaction as a superposition of P→M σ- and retrodative M→P π-bonding contributions (**III**, Chart 1), which implies a similar metal-ligand double bond character as in metal carbonyl and Fischer-type carbene complexes, respectively.[3] However, in certain cases, NHPs had also been reported to adopt an alternate coordination mode, which is characterized by an elongated M–P distance and pyramidal phosphorus coordination geometry and does not seem well in accord with metal-ligand double bonding.[4,5] Being first observed in complexes with electron rich metals, it was suggested [4] that the P→M bonding contribution can be neglected, so that the phosphenium ion acts essentially as an electrophile ("Z-type" ligand [6]) and the metal-ligand interaction becomes essentially a dative M→P-(σ-)bond (**IVa**, Chart 1).[7]

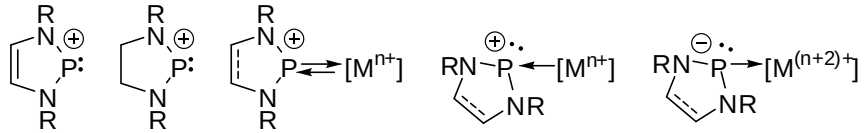

I **II** **III** **IVa** **IVb**

Chart 1. NHP Ligands and their binding modes in transition metal complexes ([M] = transition metal complex fragment; n = -1, 0).

Some time ago, Thomas et al. [8] pointed out that this view represents just one of two limiting descriptions, and that an elongated P–M distance and pyramidal phosphorus coordination geometry, which they had observed for some complexes containing a chelating NHP pincer-ligand, can likewise result from the interaction of a negatively charged "X-type" [6] phosphido ligand with

a formally oxidized metal atom (**IVb**, Chart 1). Moreover, they compared the change from a planar to a pyramidal binding mode of the NHP unit to the well-known structural dichotomy of metal-bound nitrosyls, which can adopt linear or bent geometries, and interpreted both trends as a potential implication of 'non-innocent' ligand character.[8]

The term 'non-innocent' or 'suspect' behavior of a metal coordination compound is associated with "the occurrence of situations, in which the assignment of oxidation states is not a priori obvious, because the ligands can also undergo electron transfer and thus 'ligand oxidation state' changes".[9] The NO ligand, which can formally occur as NO^+, $NO^\bullet$, or NO^-,[9] was identified as "the simplest case of a suspect ligand",[10] and extensive spectroscopic and structural studies aiming at the characterization of its bonding mode and charge state have been carried out.[11] In this context, theoretical predictions [12] and experimental studies [13,14] revealed that a linear MNO geometry does not necessarily imply nitrosonium (NO^+) character of the ligand, but may as well be compatible with a description as a nitrosyl ($NO^\bullet$) or even nitroxide (NO^-) moiety. Moreover, the assignment of well-defined metal and ligand charge states in NO-complexes is often foiled by a highly covalent character of the metal-nitrogen interaction, which renders unambiguous partitioning of electrons unfeasible.[15] As a consequence, the $M(NO)_n$ subunit in a metal complex is classified by counting only the total number *m* of electrons in the metal d-orbitals and the π*(NO)-orbitals in the form $\{M(NO)_n\}^m$ (Enemark–Feltham notation[12]), thus avoiding the assignment of specific oxidation states for the metal and ligand fragments.[16]

Apart from theoretical and conceptual issues, the 'suspect' behavior of a NO unit has impact on its chemical behavior, as a change in charge state allows switching between electrophilic and nucleophilic behavior of the ligand.[11a] A similar two-sided chemical reactivity was also noted for some NHP-complexes. Thomas and coworkers demonstrated that the addition of phenol and

thiophenol across the platinum-phosphorus double bond of cationic complex **V** proceeds with opposite regioselectivity (Scheme 1) to afford products with P–O/Pt–H and P–H/Pt–S bonds which may well be associated an electrophilic and nucleophilic (or phosphenium and phosphide) character of the NHP unit, respectively.[17] Our group has shown that the NHP-unit in the neutral manganese complex **VI** is readily attacked by nucleophiles, in accord with an electrophilic nature of the ligand,[18] whereas P-methylation of the same NHP-moiety observed during reaction of the anionic complex **VII** with methyl iodide points to its nucleophilic character.[19] Quite surprisingly, computational and spectroscopic studies on **VI**, **VII** attest the NHP-units in both complexes predominant phosphenium character.[18,19]

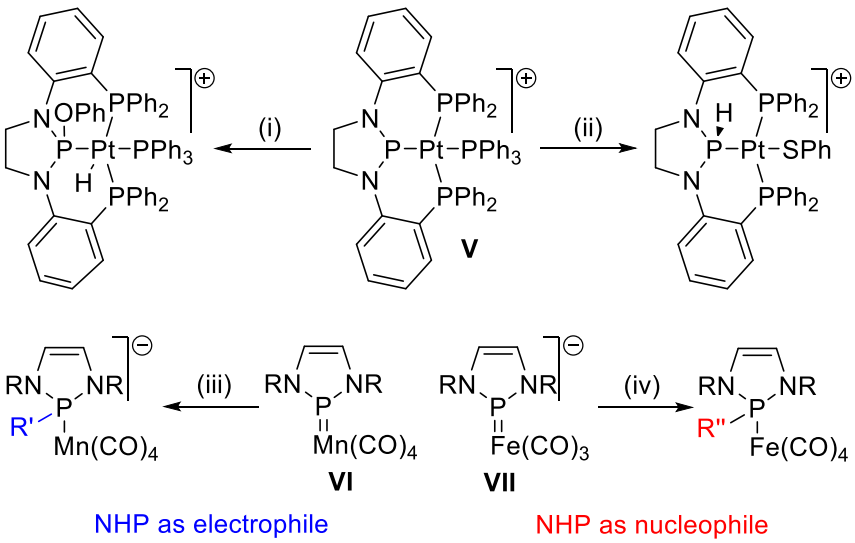

Scheme 1. Two-sided reactivity of NHP-complexes highlighting electrophilic or nucleophilic character of the phosphorus-based ligand (R = Dipp, R' = H, CH_3; R'' = CH_3). Reagents and conditions: (i) PhOH; (ii) PhSH, - PPh_3; (iii) BEt_3H^-, - BEt_3 or MeLi, - Li^+; (iv) CH_3I, CO, - I^-.

In order to substantiate the frequently drawn analogies between the coordination behavior of NHPs or other phosphenium ions on one side and NO on the other side,[3a,4,8] we considered a direct

comparison of the chemical properties of these ligands appealing. Since it is known that spectral signatures[11b,c,20] and chemical properties[11a,17-19,21] of both NO and phospheniums may vary strongly with the metal and the co-ligands present, we reckoned that meaningful results would be best obtained from an analysis of the properties of competing donor units in the same complex. Compounds featuring both NHP and NO ligands are to the best of our knowledge unknown. We report here on the first synthesis of iron and chromium complexes of this type, and present the results of structural, spectroscopic, computational and reactivity studies that cast a light on electronic properties and charge states of the N- and P-based ligands.

Experimental Section

All manipulations were carried out under an atmosphere of inert argon inside glove boxes or by using standard vacuum line techniques. Solvents were dried by literature known procedures. NMR spectra were recorded on Bruker Avance 250 or Bruker Avance 400 instruments at ambient temperature if not stated otherwise. Chemical shifts are referred to external TMS (^{1}H, ^{13}C), 85 % H_3PO_4 (Ξ = 40.480747 MHz, ^{31}P), or $SnMe_4$ (Ξ = 37.290632 MHz, ^{119}Sn), respectively. The FTIR spectra were recorded with a Thermo Scientific/ Nicolet iS5 instrument equipped with an iD5 attenuated total reflectance (ATR) accessory. Elemental analyses were determined on a Thermo Micro Cube CHN analyzer. UV/VIS spectra were recorded with a J&M TIDAS spectrophotometer. The NHP triflate **1**,[22] metallates PPN[Fe(NO)(CO)$_3$][23] and PPN[Cr(NO)(CO)$_4$][24], and H(OEt$_2$)$_2$[TRISPHAT][25] were prepared as reported elsewhere. The saturated NHP triflate **1^{sat}** was prepared from the appropriate 2-bromo-diazaphospholidine by analogy to the known procedure based on the chloro-derivative.[26]

Preparation of 4. Phosphenium salt **1** (1.11 g, 2.00 mmol) and ferrate **2** (1.42 g, 2.00 mmol)

were dissolved in thf (30 mL). The solution was stirred for 0.5 h at ambient temperature until its color had turned from yellow to red and the vigorous gas evolution had ceased. The solvent was removed under reduced pressure, the residue dispersed in n-hexane (40 mL), and filtered. The filtrate was concentrated to a volume of about 30 mL and stored for 24 h at -24 °C. The product separated as a red, crystalline solid (480 mg, 0.87 mmol, yield 44 %). ^{1}H NMR (250 MHz, C_6D_6): δ 7.25-7.04 (m, 6 H, C_6H_3), 6.36 (d, $^{3}J_{PH}$ = 5.7 Hz, 2 H, NCH), 3.09 (sept, $^{3}J_{HH}$ = 6.9 Hz, 4 H, CH), 1.37 (d, $^{3}J_{HH}$ = 6.9 Hz, 12 H, CH_3), 1.09 (d, $^{3}J_{HH}$ = 6.9 Hz, 12 H, CH_3). ^{31}P{^{1}H} NMR (101.2 MHz, C_6D_6): δ 239.1 (s). ^{13}C{^{1}H} NMR (62.9 MHz, C_6D_6): δ 218.9 (d, $^{2}J_{CP}$ = 7.8 Hz, CO), 146.3 (d, $^{3}J_{CP}$ = 3.7 Hz, *o*-C), 132.7 (d, $^{2}J_{CP}$ = 6.2 Hz, *ipso*-C), 130.2 (d, $^{5}J_{CP}$ = 1.7 Hz, *p*-C), 126.4 (d, $^{2}J_{CP}$ = 3.3 Hz, NCH), 124.3 (d, $^{4}J_{CP}$ = 1.0 Hz, *m*-C), 29.0 (s, CH), 24.7 (s, CH_3), 23.0 (s, CH_3). IR (solid): $\tilde{\nu}$ [cm^{-1}] = 1981 (s), 1921 (s) *v*CO, 1698 (s) *v*NO. IR (n-hexane): $\tilde{\nu}$ [cm^{-1}] = 2000 (m), 1951 (m) *v*CO, 1735 (m) *v*NO. UV-VIS (MeCN, $c = 4.0 \cdot 10^{-5}$ M): λ_{max} [nm] (ε_{max} [l mol^{-1} cm^{-1}]) 366 (6600), 450 (sh). $C_{28}H_{36}FeN_3O_3P$ (549.43): calcd C 61.21, H 6.60, N 7.65; found C 61.35, H 6.65, N 7.59.

Preparation of 4^{sat}. The reaction of phosphenium salt **1^{sat}** (0.56 g, 1.00 mmol) and ferrate **2** (0.71 g, 1.00 mmol) in thf (15 mL) and the work-up of the reaction mixture was carried out as described for **1**. The product was obtained as an orange, crystalline solid (50 mg, 0.09 mmol, yield 9 %). Even if no satisfactory elemental analysis could be obtained, the product was found to be spectroscopically pure. ^{1}H NMR (400 MHz, C_6D_6): δ 7.23-7.05 (m, 6 H, C_6H_3), 3.50 (d, $^{3}J_{PH}$ = 4.2 Hz, 4 H, NCH_2), 3.38 (sept, $^{3}J_{HH}$ = 6.8 Hz, 4 H, CH), 1.42 (d, $^{3}J_{HH}$ = 6.8 Hz, 12 H, CH_3), 1.18 (d, $^{3}J_{HH}$ = 6.8 Hz, 12 H, CH_3). ^{31}P{^{1}H} NMR (161.9 MHz, C_6D_6): δ 281.4 (s). ^{13}C{^{1}H} NMR (100.5 MHz, C_6D_6): δ 221.3 (d, $^{2}J_{CP}$ = 7.8 Hz, CO), 149.9 (d, $^{3}J_{CP}$ = 2.9 Hz, *o*-C), 135.3 (d, $^{2}J_{CP}$ = 8.4 Hz, *ipso*-C), 131.8 (br, *p*-C), 126.2 (br, *m*-C), 56.0 (d, $^{2}J_{CP}$ = 3.1 Hz, NCH_2), 31.4 (s, CH), 27.5 (s, CH_3), 26.1 (s, CH_3). IR (solid): $\tilde{\nu}$ [cm^{-1}] = 1987 (s), 1974 (s), 1928 (s), 1916 (s) *v*CO; 1728 (s),

1698 (s) *v*NO. IR (thf): $\tilde{\nu}$ [cm^{-1}] = 1994 (m), 1940 (m) *v*CO; 1724 (m) *v*NO. UV-VIS (MeCN, *c* = 1.9 $\cdot 10^{-4}$ M): λ_{max} [nm] (ε_{max} [l mol^{-1} cm^{-1}]) 345 (2200), 420 (sh).

Preparation of 5. The reaction of phosphenium salt **1** (0.56 g, 1.00 mmol) and chromate **3** (0.74 g, 1.00 mmol) in thf (15 mL) was carried out as described for **4**. The residue obtained after removal of the solvent under reduced pressure was extracted with n-hexane (40 mL). The resulting dispersion was filtered and the filtrate concentrated to a volume of about 20 mL. Storage at -24 °C for 24 h produced a deep red, crystalline solid (270 mg, 0.47 mmol, yield 47 %). ^{1}H NMR (250 MHz, C_6D_6): δ 7.28-7.06 (m, 6 H, C_6H_3), 6.18 (d, $^{3}J_{PH}$ = 7.3 Hz, 2 H, NCH), 3.16 (sept, $^{3}J_{HH}$ = 6.9 Hz, 4 H, CH), 1.32 (d, $^{3}J_{HH}$ = 6.9 Hz, 12 H, CH_3), 1.11 (d, $^{3}J_{HH}$ = 6.9 Hz, 12 H, CH_3). ^{31}P{^{1}H} NMR (101.2 MHz, C_6D_6): δ 269.8 (s). ^{13}C{^{1}H} NMR (62.9 MHz, C_6D_6): δ 231.1 (d, $^{2}J_{CP}$ = 15.6 Hz, CO), 146.7 (d, $^{3}J_{CP}$ = 2.5 Hz, *o*-C), 132.5 (d, $^{2}J_{CP}$ = 6.0 Hz, *ipso*-C), 129.6 (d, $^{5}J_{CP}$ = 1.5 Hz, *p*-C), 124.9 (d, $^{2}J_{CP}$ = 1.8 Hz, NCH), 123.9 (d, $^{4}J_{CP}$ = 1.3 Hz, *m*-C), 28.1 (s, CH), 23.7 (s, CH_3), 22.2 (s, CH_3). IR (solid): $\tilde{\nu}$ [cm^{-1}] = 2016 (m), 1951 (m) 1931 (s) *v*CO; 1664 (s) *v*NO. IR (n-hexane): $\tilde{\nu}$ [cm^{-1}] = 2025 (m), 1968 (m) *v*CO; 1688 (m) *v*NO. $C_{29}H_{36}CrN_3O_4P$ (573.59): calcd C 60.73, H 6.33, N 7.33; found C 60.84, H 6.43, N 7.22.

Preparation of 5^{sat}. The reaction of phosphenium salt **1^{sat}** (0.38 g, 0.68 mmol) and chromate **3** (0.60 g, 0.82 mmol) in thf (10 mL) was carried out as described for **4**. The residue obtained after removal of the solvent under reduced pressure was extracted with n-hexane (30 mL). The resulting dispersion was filtered and the filtrate was concentrated to a volume of about 15 mL. Storage at -24 °C for 24 h produced 55 mg (0.10 mmol, yield 14 %) of an orange-red, crystalline solid. The product used for analytical characterization contained a minor amount of hydrolysis product **10** which could not be separated by fractional recrystallization due to similar solubilities. ^{1}H NMR (250 MHz, C_6D_6): δ 7.29-7.01 (m, 6 H, C_6H_3), 3.42 (d, $^{3}J_{PH}$ = 3.5 Hz, 4 H, NCH), 3.33 (sept, $^{3}J_{HH}$

= 6.9 Hz, 4 H, CH), 1.35 (d, $^{3}J_{HH}$ = 6.9 Hz, 12 H, CH_3), 1.18 (d, $^{3}J_{HH}$ = 6.9 Hz, 12 H, CH_3). $^{31}P\{^{1}H\}$ NMR (101.2 MHz, C_6D_6): δ 303.3 (s). $^{13}C\{^{1}H\}$ NMR (62.9 MHz, C_6D_6): δ 230.1 (d, $^{2}J_{CP}$ = 17.8 Hz, CO), 148.6 (d, $^{3}J_{CP}$ = 2.2 Hz, *o*-C), 134.3 (d, $^{2}J_{CP}$ = 8.1 Hz, *ipso*-C), 129.7 (d, $^{5}J_{CP}$ = 1.5 Hz, *p*-C), 124.9 (d, $^{4}J_{CP}$ = 1.2 Hz, *m*-C), 53.9 (d, $^{2}J_{CP}$ = 2.0 Hz, NCH_2), 28.9 (s, CH), 25.0 (s, CH_3), 23.7 (s, CH_3). IR (solid): $\tilde{\nu}$ [cm^{-1}] = 2023 (m), 1958 (m) 1929 (s) *v*CO; 1656 (s) *v*NO. IR (thf): $\tilde{\nu}$ [cm^{-1}] = 2029 (w), 1966 (m) *v*CO, 1678 (m) *v*NO. $C_{29}H_{36}CrN_3O_4P$ (575.61): calcd C 60.51, H 6.65, N 7.30; found C 62.75, H 7.57, N 6.79.

Preparation of PPh_4[6]. A 1 M solution of $LiHBEt_3$ in thf (0.28 mL, 0.28 mmol) was added to a solution of **4** (140 mg, 0.25 mmol) in Et_2O (10 mL). The mixture was stirred for 20 h at ambient temperature. During this time, the color changed from red to yellow. PPh_4Cl (140 mg, 38 mmol) was added, and the suspension formed was stirred for additional 20 h. The yellow precipitate was filtered off and subsequently extracted with toluene (40 mL). Storage of the yellow-orange extract at -24 °C for 24 h afforded 95 mg (0.11 mmol, yield 43 %) of a yellow, crystalline solid that was found to be spectroscopically pure. ^{1}H NMR (250 MHz, C_6D_6): δ 9.32 (d, $^{1}J_{PH}$ = 286 Hz, 1 H, PH), 7.38-7.00 (m, 26 H, C_6H_3 and C_6H_5), 6.23 (d, $^{3}J_{PH}$ = 5.5 Hz, 2 H, NCH), 4.21 (sept, $^{3}J_{HH}$ = 6.8 Hz, 2 H, CH), 3.79 (sept, $^{3}J_{HH}$ = 6.7 Hz, 2 H, CH), 1.70 (d, $^{3}J_{HH}$ = 6.8 Hz, 6 H, CH_3), 1.53 (d, $^{3}J_{HH}$ = 6.7 Hz, 6 H, CH_3), 1.48 (d, $^{3}J_{HH}$ = 6.8 Hz, 6 H, CH_3), 1.36 (d, $^{3}J_{HH}$ = 6.7 Hz, 6 H, CH_3). ^{31}P NMR (101.2 MHz, C_6D_6): δ 139.6 (d, $^{1}J_{PH}$ = 286 Hz), 22.3 (br). A satisfying ^{13}C NMR spectrum could not be obtained due to low solubility. IR (solid): $\tilde{\nu}$ [cm^{-1}] = 1897 (s), 1820 (s) *v*CO; 1622 (s) *v*NO; 2066 (w) *v*PH. $C_{52}H_{57}FeN_3O_3P_2$ (889.84): calcd C 70.19, H 6.46, N 4.72; found C 67.29, H 6.32, N 4.45. The low carbon content found in the microanalysis is presumably due to carbide formation during the combustion process. The spectroscopic data reveal no detectable impurity.

Preparation of PPh_4[8]. The reaction of a solution of **4** (110 mg, 0.20 mmol) in Et_2O (10 mL) with MeLi (0.14 mL of a 1.6 M soln. in Et_2O, 0.22 mmol) and PPh_4Cl (100 mg, 30 mmol) was carried out as described for PPh_4[**6**]. Storage of the yellow-orange extract at -24 °C for 24 h gave 85 mg (0.09 mmol, yield 47 %) of an orange, crystalline solid. ^{1}H NMR (400 MHz, thf-d_8): δ 9.83 (d, 1 H, $^1J_{PH}$ = 286 Hz, PH), 7.94-7.66 (m, 20 H, C_6H_3 and C_6H_5), 7.27-7.06 (m, 6 H, C_6H_3 and C_6H_5), 5.87 (d, $^3J_{PH}$ = 4.7 Hz, 2 H, NCH), 3.97 (sept, $^3J_{HH}$ = 6.6 Hz, 2 H, CH), 3.77 (sept, $^3J_{HH}$ = 6.7 Hz, 2 H, CH), 1.47 (s, 3 H, PCH_3), 1.33 (d, $^3J_{HH}$ = 6.6 Hz, 6 H, CH_3), 1.29 (d, $^3J_{HH}$ = 6.6 Hz, 6 H, CH_3), 1.24 (d, $^3J_{HH}$ = 6.6 Hz, 6 H, CH_3), 1.10 (d, $^3J_{HH}$ = 6.6 Hz, 6 H, CH_3). ^{31}P NMR (161.9 MHz, thf-d_8): δ 168.9 (s), 24.0 (br). A satisfying ^{13}C NMR spectrum could not be obtained due to low solubility. IR (solid): $\tilde{\nu}$ [cm^{-1}] = 1888 (s), 1810 (s) νCO; 1604 (s) νNO. $C_{53}H_{59}FeN_3O_3P_2$ (903.84): calcd C 70.43, H 6.58, N 4.65; found C 70.04, H 6.61, N 4.64.

Reaction of 4 with NaN_3. A solution of **4** (110 mg, 0.20 mmol), NaN_3 (13 mg, 0.20 mmol) and catalytic amounts of LiCl in thf was stirred for 10 h at 60 °C. A ^{31}P NMR spectrum of the reaction mixture (161.9 MHz, thf) showed the resonances of 2-azido diazaphospholene **9**[27] (δ ^{31}P = 119.0 ppm) and secondary diazaphospholene oxide **10**[28] (δ ^{31}P = 4.8 ppm), which were identified by comparison with authentic samples. No attempt to work-up was made.

Reaction of PPh_4[6] with $H(OEt_2)_2$[TRISPHAT]. PPh_4[**6**] (25 mg, 30 µmol) and $H(OEt_2)_2$[TRISPHAT] (26 mg, 30 µmol) were dissolved in toluene (5 mL). The solution was stirred for 20 h at ambient temperature. During this time, the color changed from yellow to orange, and a colorless precipitate formed. Filtration and removal of the solvent from the filtrate afforded an orange-red oil which was characterized by ^{31}P NMR spectroscopy. ^{31}P NMR (161.9 MHz, C_6D_6): δ -80.0 (s, TRISPHAT$^-$), 22.5 (br, PPh_4^+), 239.1 (s, **4**), 126.9 (d, $^1J_{PH}$ = 307 Hz, unidentified), 137.6 (d, $^1J_{PH}$ = 346 Hz, unidentified).

Reaction of 4^{sat} with $LiBEt_3H$/Et_3NHCl. Excess $LiBEt_3H$ (50 µl of a 1 M solution in thf) was added to a solution of $\mathbf{4^{sat}}$ (20 mg, 36 µmol) in Et_2O (0.4 mL) in an NMR tube. Formation of Li[$\mathbf{6^{sat}}$] was verified by ^{31}P NMR spectroscopy ($\delta^{31}P$ = 132.3 (d, $^1J_{PH}$ = 296 Hz)). Solid Et_3NHCl was added. A ^{31}P NMR spectrum indicated formation of a mixture with $\mathbf{4^{sat}}$ as main product. ^{31}P NMR (101.2 MHz, Et_2O): δ 279.7 (s, $\mathbf{4^{sat}}$), 136.6 (d, $^1J_{PH}$ = 348 Hz, unidentified), 122.4 (d, $^1J_{PH}$ = 303 Hz, unidentified), 8.4 (s, unidentified), 5.0 (d, $^1J_{PH}$ = 607 Hz, **10**).

Reaction of 5 with $LiBEt_3H$ and Et_3NHCl. A 1 M solution of $LiBEt_3H$ in thf (0.13 mL, 0.13 mmol) was added to a solution of **5** (50 mg, 90 µmol) in Et_2O (5 mL). The mixture was stirred for 1 h at ambient temperature and the solvent removed under reduced pressure. Formation of Li[**7**] was verified by NMR spectroscopy (^{31}P NMR (101.2 MHz, C_6D_6): δ = 155.6 (d, $^1J_{PH}$ = 301 Hz); ^1H,^{31}P HMQC (250 MHz, C_6D_6): δ = 9.58 (d, $^1J_{PH}$ = 301 Hz, PH)). For the reaction with Et_3NHCl, a new ethereal solution of **Li[7]** was prepared as described. Solid Et_3NHCl (25 mg, 0.18 mmol) was added and the mixture stirred for 1 h during which its color turned from deep-red to yellow. The mixture was filtered and the filtrate evaporated under reduced pressure to produce crude **11** as a yellow solid which could not be further purified. Selected spectral data: ^1H NMR (250 MHz, C_6D_6): δ = 8.84 (dd, $^1J_{PH}$ = 312 Hz, $^3J_{HH}$ = 2.2 Hz, 1 H, PH), 7.29-6.97 (m, 6 H, C_6H_3), 5.89 (d, $^3J_{PH}$ = 8.1 Hz, 2 H, NCH), 3.50 (sept, $^3J_{HH}$ = 6.9 Hz, 2 H, CH), 3.18 (sept, $^3J_{HH}$ = 6.9 Hz, 2 H, CH), 1.38 (d, $^3J_{HH}$ = 6.9 Hz, 6 H, CH_3), 1.31 (d, $^3J_{HH}$ = 6.9 Hz, 6 H, CH_3), 1.21-1.13 (m, 12 H, CH_3) - 4.93 (dd, $^2J_{PH}$ = 55 Hz, $^3J_{HH}$ = 2.2 Hz, 1 H, CrH). ^{31}P NMR (101.2 MHz, C_6D_6): δ = 134.0 (dd, $^1J_{PH}$ = 312 Hz, $^2J_{PH}$ = 55 Hz). IR (solid): $\tilde{\nu}$ [cm^{-1}] = 2138 (w), νPH; 2066 (m), 1991 (s), 1960 (m), 1924 (m), νCO; 1710 (s), νNO.

Reaction of 5^{sat} with $LiBEt_3H$ and Et_3NHCl. Excess $LiBEt_3H$ (50 µl of a 1 M solution in thf)

was added to a solution of **5**^{sat} (20 mg, 35 µmol) in C_6D_6 (0.4 mL) in an NMR tube. ^{31}P and $^{1}H,^{31}P$ HMQC NMR spectra (250/101.2 MHz) confirmed the formation of Li[**7**^{sat}] ($\delta^{31}P$ = 147.4 (d, $^{1}J_{PH}$ = 298 Hz); $\delta^{1}H$ = 9.17 (d, $^{1}J_{PH}$ = 298 Hz), PH). Addition of solid Et_3NHCl led to a color change from deep red to yellow, and ^{31}P NMR spectroscopic survey indicated the formation of **11**^{sat}. Selected NMR data: ^{31}P NMR (101.2 MHz, C_6D_6): δ = 127.9 (dd, $^{1}J_{PH}$ = 310 Hz, $^{2}J_{PH}$ = 52 Hz). $^{1}H,^{31}P$ HMQC (250 MHz, C_6D_6): δ = 8.27 (br d, $^{1}J_{PH}$ = 310 Hz, 1 H, PH), -5.23 (dd, $^{2}J_{PH}$ = 52 Hz, $^{3}J_{HH}$ = 1.9 Hz, 1 H, CrH).

Preparation of 12. PPh_4**[6]** (150 mg, 0.17 mmol) and Ph_3SnCl (65 mg, 0.17 mmol) were dissolved in benzene (10 mL). The solution was stirred for 2 h at ambient temperature, the solvent removed under reduced pressure, and the residual yellow solid extracted with n-hexane (20 mL) and filtered. Storage of the filtrate at -24 °C for 24 hours gave 40 mg (30 µmol, yield 26 %) of a yellow, crystalline solid. ^{1}H NMR (250 MHz, C_6D_6): δ 9.66 (d, $^{1}J_{PH}$ = 335 Hz, 1 H, PH), 7.90-7.60 (m, 6 H, *o*-C_6H_5) 7.25-6.95 (m, 15 H, C_6H_3 and *m/p*-C_6H_5), 5.99 (d, $^{3}J_{PH}$ = 10.7 Hz, 2 H, NCH), 3.67 (sept, $^{3}J_{HH}$ = 6.8 Hz, 2 H, CH), 3.36 (sept, $^{3}J_{HH}$ = 6.7 Hz, 2 H, CH), 1.35 (d, $^{3}J_{HH}$ = 6.8 Hz, 6 H, CH_3), 1.25-1.14 (m, 18 H, CH_3). ^{31}P NMR (101.2 MHz, C_6D_6): δ 133.6 (dt, $^{1}J_{PH}$ = 335 Hz, $^{3}J_{PH}$ = 11 Hz, $^{2}J_{P^{119}Sn}$ = 98 Hz). ^{119}Sn NMR (93.2 MHz, C_6D_6): δ 48.4 (d, $^{2}J_{P^{119}Sn}$ = 98 Hz). $^{13}C\{^{1}H\}$ NMR (62.9 MHz, C_6D_6): δ 208.6 (d, $^{2}J_{CP}$ = 19.9 Hz, CO), 148.5 (d, $^{3}J_{CP}$ = 2.9 Hz, *o*-C), 148.2 (d, $^{3}J_{CP}$ = 1.7 Hz, *o*-C), 140.8 (d, $^{5}J_{CP}$ = 1.5 Hz, *p*-C), 135.9 (s, *o*-Ph), 133.8 (d, $^{2}J_{CP}$ = 5.5 Hz, *ipso*-C), 128.3 (d, $^{4}J_{CP}$ = 1.6 Hz, *m*-C), 127.9 (s, *p*-Ph), 127.6 (s, *m*-Ph), 123.6 (s, *ipso*-Ph), 123.3 (d, $^{4}J_{CP}$ = 1.4 Hz, *m*-C), 121.4 (broad s, NCH), 28.9 (s, CH), 27.8 (s, CH), 25.5 (s, CH_3), 23.6 (s, CH_3), 22.0 (s, CH_3), 21.7 (s, CH_3). IR (solid): $\tilde{\nu}$ [cm^{-1}] = 1987 (m), 1932 (s), *ν*CO; 1731 (s), *ν*NO; 2154 (w), *ν*PH. Anal. Calcd for $C_{46}H_{51}FeN_3O_3PSn$ (899.46): C 61.43, H 5.72, N 4.67 Found: C 61.13, H 5.76, N 4.69.

Crystallographic Studies. Single-crystal X-ray diffraction data were measured with a Bruker Kappa APEX2 Duo diffractometer at 100(2) K for **4**, PPh_4[**6**] and PPh_4[**8**], and at 130(2) K for $\mathbf{4}^{sat}$, **5**, $\mathbf{5}^{sat}$ and **12**, respectively, using Mo K_α radiation (λ = 0.71073 nm) for PPh_4[**6**], PPh_4[**8**], **4**, $\mathbf{4}^{sat}$, **5** and **12**, and Cu K_α-radiation (λ = 1.54178 nm) for $\mathbf{5}^{sat}$. The structures were solved by direct methods (SHELXS-2014[29]) and refined with a full-matrix-least-squares scheme on F^2 (SHELXL-2014[29]). Semi-empirical absorption corrections from equivalents were applied in all cases. Non-hydrogen atoms were refined anisotropically. The disordered CO/NO atoms in **4**, **5** and $\mathbf{5}^{sat}$ and the additional disordered carbon atoms in $\mathbf{4}^{sat}$ and $\mathbf{5}^{sat}$ were refined isotropically. PPh_4[**6**] and PPh_4[**8**] co-crystallize with one molecule of toluene without any disorder. PPh_4[**8**] crystallized as a non-merohedral twin, which led to a poor data quality. Further crystallographic data and details on the structure solution are given in the Supporting Information. CCDC-1893312 (**4**), CCDC-1893311 ($\mathbf{4}^{sat}$), CCDC-1893310 ($\mathbf{5}^{sat}$), CCDC-1893308 (**5**), 1893306 (PPh_4[**6**]), CCDC-1893307 (PPh_4[**8**]) and CCDC-1893309 (**12**) contain the crystallographic data for this paper, which can be obtained free of charge from the Cambridge Crystallographic Data Centre via www.ccdc.cam.ac.uk/data_request/cif.

Electrochemical studies. Cyclic voltammetry was performed with a EG&Princeton Applied Research M273A potentiostat equipped with a M175 function generator, using a three-electrode configuration (Pt working and counter electrodes, Ag wire reference electrode) in thf/0.1 M NBu_4OTf solution at a scan rate of 100 mV/s. Fc/Fc^+ was used as an internal reference. IR-spectroelectrochemistry was carried out with a PGSTAT101 potentiostat by Methrom Autolab B.V. and a Thermo Scientific Nicolet 6700 FT-IR spectrometer using an optically transparent thin layer electrochemical (OTTLE) cell.[30] EPR spectra were recorded with a Magnetech MiniScope MS5000 EPR spectrometer in the X-band (9.5 GHz). The samples were prepared by electrolysis

of a 0.02 M solution of **4** in thf/0.2 M NBu_4OTf at a constant voltage of 2.5 V.

Computational Studies. All calculations were carried out with the Gaussian 09 program package.[31] Full geometry optimization was performed for all molecules at the DFT level using the B3LYP [32] and ωB97xD [33] functionals with aug-cc-pVDZ [34] basis sets. Harmonic vibrational frequency calculations were carried out at the same levels to establish the nature of the stationary points obtained as local minima (only positive normal modes) or transition states (one imaginary normal mode). Standard Gibbs free energies ΔG_0 were obtained using the calculated harmonic frequencies. The UωB97xD/aug-cc-pVDZ (for **4**/**4**^{sat}) and RωB97xD/aug-cc-pVDZ results (for **5**/**5**^{sat}) were used for the discussion. NBO population analyses were carried out using the NBO6.0 program.[35] Single point CASPT2(n,n)/cc-pVDZ calculations for neutral **H-4** (with n = 4) and radical anion {**H-4**}$^{\bullet-}$ (with n = 5) were carried out at the DFT-optimized geometries using two metal d-orbitals, the π*(NO) orbitals, and – for {**H-4**}$^{\bullet-}$ – a π*(NPN) orbital centered on the NHP fragment as the active space. Electronic spectra and natural transition orbitals [36] for **Me-4**/**Me-4**^{sat} were computed at the TD-RCAM-B3LYP/aug-cc-pVTZ level of theory at the UωB97xD/aug-cc-pVDZ geometries. The GABEDIT program [37] was used for visualization.

Results and Discussion

Complex synthesis and characterization. The complexes **4**, **5** and **4**^{sat}, **5**^{sat} (Scheme 2) are accessible by salt metathesis between 'unsaturated' (**1**[OTf]), type I in chart 1) or 'saturated' (**1**^{sat}[OTf], type II) NHP triflates and equimolar amounts of metallates **2**, **3**, respectively. Complexes **4**, **5** with 'unsaturated' ligands were isolated in reasonable yields (44-47%), whereas the yields of **4**^{sat} and **5**^{sat} were poor (9-14%), as the reactions were less selective and the work-up suffered from high losses during recrystallization. The iron complexes are moderately air stable as

solids and chemically quite robust in solution, whereas the chromium complexes decomposed slowly both in solution and in the solid state.

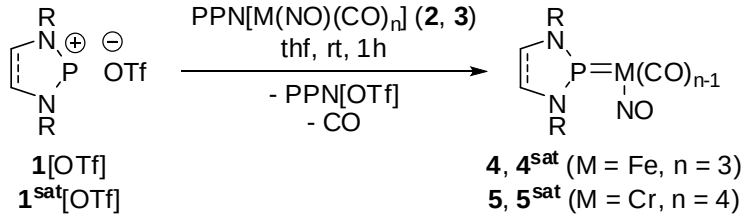

Scheme 2. Preparation of complexes **4**, **4**^{sat}, **5**, **5**^{sat} (OTf^- = $F_3CSO_3^-$; R = 2,6-*i*$Pr_2C_6H_3$ (Dipp); PPN = bis(triphenylphosphine)iminium; M = Fe, n = 3 for **2**, **4**, **4**^{sat}; M = Cr, n = 4 for **3**, **5**, **5**^{sat}).

All complexes were characterized by NMR and IR spectroscopy and single-crystal X-ray diffraction studies. The ^{31}P NMR spectra display signals at high chemical shifts (see Table 1), which match those of known NHP complexes of iron[2,19] and chromium,[18b,38] respectively.

Table 1. Selected spectroscopic data of iron and chromium carbonyl nitrosyl complexes**.**

Complex	δ^{31}P (C_6D_6) [ppm]	νNO [cm^{-1}]	νCO [cm^{-1}]
4	239.1	1735 [a]	2000, 1951 [a]
4^{sat}	281.4	1724 [b]	1994, 1940 [b]
5	269.8	1688 [a]	2025, 1968 [a]
5^{sat}	303.3	1678 [b]	2029, 1966 [b]
$Na[Fe(NO)(CO)_3]$ [c]	-	1646	1978, 1875
$PPN[Cr(NO)(CO)_4]$ [d]	-	1608	1993, 1895, 1850
[**4**$^{\bullet-}$] [e]	-	1610	1909, 1833

[a] in n-hexane. [b] in thf. [c] data from ref. 39. [d] data from ref. 24. [e] in situ generated by electrochemical reduction of **4** in thf.

The molecular structures confirm this similarity by revealing that complexes **4**, **4**^{sat} (Figure 1) and **5**, **5**^{sat} (Figure 2) exhibit, like their congeners,[19,38,40] trigonal planar coordinated phosphorus

atoms (sum of bond angles at P: 359.7(2) to 360.0(6)°). The Fe–P distance in complex **4** (2.0331(5) Å) is marginally shorter than in **4**^{sat} (2.0291(6) Å), and both values are intermediate between those for previously reported iron carbonyl complexes derived from **1**$^{+}$ (1.989(1) Å for ([(**1**)Fe(CO)$_3$][PPh$_4$] to 2.011(1) Å for [(**1**)Fe(CO)$_3$H] [19]) and a cationic complex with an acyclic diaminophosphenium ligand (2.10(5) Å for [{(Et$_2$N)$_2$P}Fe(CO)$_4$][AlCl$_4$][40]). The Cr–P distances in **5** (2.1360(16) Å) and **5**^{sat} (2.1345(14) Å) are indistinguishable within experimental error and slightly exceed those in the only other structurally characterized phosphenium complex of chromium (Cr–P 2.1130(4), 2.1179(4) Å for [(^{tms}NHP)$_2$Cr(CO)$_3$]; ^{tms}NHP = 1,3-bis-Dipp-4-Me$_3$Si-diazaphospholenium [18b]). Altogether, these comparisons clearly justify assigning the metal-phosphorus bonds in **4**/**4**^{sat} and **5**/**5**^{sat} as formal double bonds, and describing these species therefore as further examples of 'Fischer carbene analogue' [3e,f] phosphenium complexes.

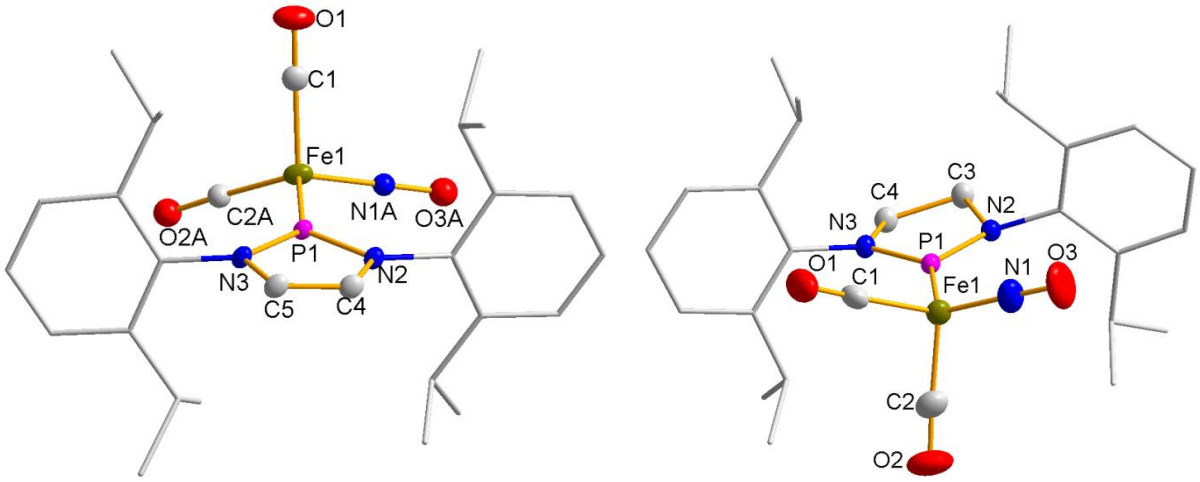

Figure 1. View of the molecular structures of **4** (left) and **4**^{sat} (right) in the crystal. For clarity, hydrogen atoms were omitted and Dipp-substituents represented using a wire model. Thermal ellipsoids were drawn at the 50 % probability level. The NO and one carbonyl ligand of **4** are disordered; for clarity, only one of the two possible orientations is shown. Selected distances [Å] and angles [°] are listed in Table 2.

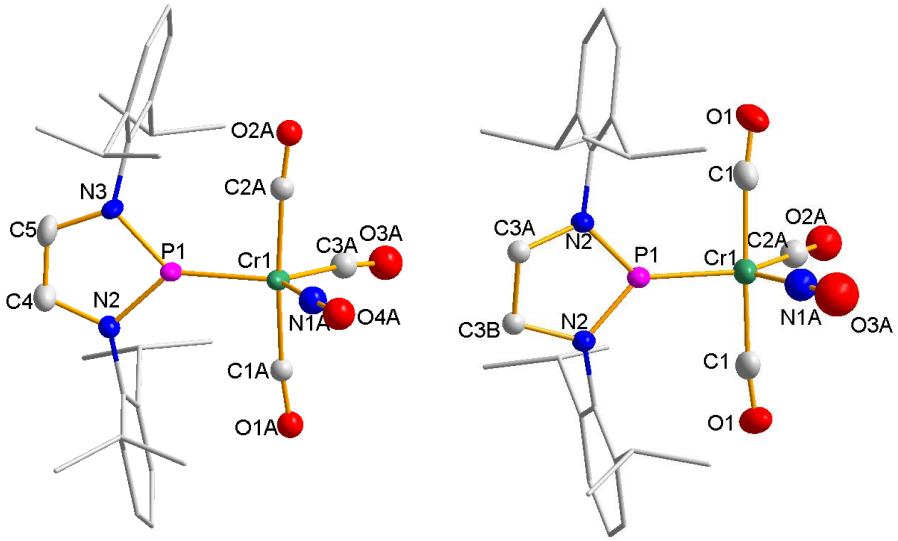

Figure 2. View of the molecular structures of **5** (left) and **5**^{sat} in the crystal. For clarity, hydrogen atoms were omitted and Dipp-substituents represented using a wire model. Thermal ellipsoids were drawn at the 50 % probability level. In case of **5**, all NO and CO ligands as well as a part of the Dipp-substituents are disordered. In case of **5**^{sat}, the equatorial NO and CO ligands as well as the methylene carbon atoms in the NHP ring are disordered. In both cases, only one orientation of the molecule is shown, and metric parameters in the disordered parts are not discussed. A detailed description of the disorder is included in the cif-files. Selected distances [Å] and angles [°] are listed in Table 2.

Table 2. Selected interatomic distances (in Å) and angles (in °) of complex iron and chromium carbonyl nitrosyls**.**

Complex	**4** (M = Fe)	**4sat** (M = Fe)	**5** (M = Cr)	**5sat** (M = Cr)	PPh_4[**6**] [a] (M = Fe)	**12** [b] (M = Fe)
M–P	2.0331(5)	2.0291(6)	2.1360(16)	2.1345(14)	2.1339(9)	2.1755(12)
M–N1		1.665(2)			1.702(3)	1.673(4)
N1–O3		1.174(3)			1.174(3)	1.182(4)

M–C1	1.801(2)	1.788(2)	1.909(4) [c]	1.758(3)	1.777(4)
M–C2		1.795(3)		1.721(4)	1.788(4)
C1–O1	1.147(3) [d]	1.143(3)	1.143(4) [c]	1.168(3)	1.152(4)
C2–O2		1.145(3)		1.167(4)	1.151(4)
P1–N2	1.6671(16)	1.6550(17)	1.647(3) [e]	1.706(3)	1.686(3)
P1–N3	1.6778(15)	1.6443(18)		1.707(2)	1.689(3)
M–N1–O3		178.6(2)		177.4(3)	179.2(3)
M–C1–O1	177.77(19)	178.0(2)	173.7(3) [c]	177.9(3)	177.4(4)
M–C2–O2		177.3(3)			177.8(4)
Σ<(P) [f]	359.91(23)	359.69(20)	359.58(36)	339.07(30)	334.78(37)

[a] further data for PPh_4[**6**]: P1–H1 1.40(2); sum of H–P–N and N–P–N bond angles 311(3)°. [b] further data for **12**: Fe1–Sn1 2.5902(6), P1–H1 1.35(3), P1–Fe1–Sn1 172.71(4), 302(3). [c] CO ligand in trans-OC–M–CO unit. [d] perpendicular to NHP plane. [e] second P–N distance equal due to crystallographic C_2-symmetry. [f] sum of M–P–N and N–P–N bond angles around P.

The metal atoms in **4**/**4**^{sat} and **5**/**5**^{sat} display distorted tetrahedral (Fe) or trigonal bipyramidal (Cr) coordination, respectively. The NO and one CO ligand in **4** are disordered over two sites in the $Fe(CO)_2(NO)$ moiety, while the third site (oriented perpendicular to the NHP ring) is exclusively occupied by a carbonyl (see Figure 1). In **5**/**5**^{sat}, a similar NO/CO disorder affects the equatorial sites in the trigonal bipyramid that are not occupied by the NHP ligand (see Figure 2). While a concise analysis of metric parameters in the disordered $\{M(CO)_n(NO)\}$ subunits remained unfeasible, the available data allow us nonetheless to rule out the presence of bent MNO-units and describe their geometry in all three species accordingly as (quasi)linear. Structural dilemmas associated with the site assignment of ligands in mixed CO/NO complexes are common,[39] even if ordered structures have been observed as well.[41] This is also the case for the remaining complex **4**^{sat}, where the linearity of the MNO unit (Fe1–N1–O3 178.6(2)°) is clearly evident in the absence of positional disorder. This geometry is in accord with the Enemark and Feltham model,[12] if one considers that the MNO-fragments in **4**/**4**^{sat} and **5**/**5**^{sat} are isoelectronic to those in $[Fe(CO)_3(NO)]^-$ and $[Cr(CO)_4(NO)]^-$ and represent thus likewise $\{FeNO\}^{10}$ and $\{CrNO\}^8$ moieties. It should be

noted that the model anticipates also the preferred coordination of the NO unit to an equatorial site of a trigonal bipyramid as observed for **5**/**5**^{sat}.

The absence of positional disorder in crystalline **4**^{sat} permits further the precise evaluation of Fe–N (1.665(2) Å) and N–O (1.174(3) Å) distances, which are similar or somewhat shorter, respectively, than those reported[41] for Tl[$Fe(CO)_3(NO)$] (Fe–N 1.659(11), N–O 1.212(14) Å). With reference to the view of the Hieber anion $[Fe(CO)_3(NO)]^-$ as a nitroxide (NO^-) complex,[14] the N–O bond shortening in **4**^{sat} is readily explained by assuming that formal replacement of one CO by a positively charged and more strongly π-accepting NHP ligand[3] reduces the negative excess charge on the nitroxide unit and thereby strengthens the N–O bond. On the other hand, the N–O distance in **4**^{sat} still exceeds that of free NO (1.154 Å), indicating that the NO bond order is closer to a double than a triple bond, and the nitroxide character is not completely overturned.

Further insight into the interaction of the NHP and NO ligands is available from the vibrational spectra of **4**/**4**^{sat} and **5**/**5**^{sat}. The νNO and νCO modes display a general blue shift with respect to those of $[Fe(CO)_3(NO)]^-$ [14,39] and $[Cr(CO)_4(NO)]^-$ [24] (Table 1), which reflects the known effect of increased π-acceptor capacity and higher positive charge of the NHP ligands compared to CO.[3] The slightly, but consistently larger shifts observed for **4**/**5** in relation to **4**^{sat}/**5**^{sat} are in accord with a higher overall π-acidity of the 'unsaturated' (type I) compared to the 'saturated' (type II) NHP ligand, which had already been noted earlier.[42] The blue shift of the νNO mode of some 80-90 cm^{-1} for **4**/**5** and 70-80 cm^{-1} for **4**^{sat}/**5**^{sat} is lower than the value of 100 cm^{-1} attributed to the effect of a unit increase in the charge of the whole complex, but certainly larger than the 10 cm^{-1} expected upon formal replacement of a carbonyl by a neutral electron accepting phosphine like PF_3.[11b,c] If one considers that the wavenumbers of the νNO modes in **4**, **5** are still significantly below the average values for the neutral 'reference' complexes $[Fe(CO)_2(NO)_2]$ (1796 cm^{-1}) and $[Cr(NO)_4]$

(approx. 1750 cm^{-1}),[11b] not to mention free NO (1875 cm^{-1}) or NO^+ (2377 cm^{-1}),[11c] the observed spectral data corroborate the conclusions drawn from the crystallographic studies that the influence of the NHP ligand in **4**/**4**^{sat} and **5**/**5**^{sat} reduces the anion character of the NO ligand, but does not switch the nitroxide into a positively charged nitrosonium unit. Vice versa, the decrease in cationic charge on the NHP fragment is probably insufficient to bring a pronounced phosphide character to the fore.

The UV-VIS spectra of **4** and **4**^{sat} exhibit broad bands with maxima at 366 nm (**4**) or 345 nm (**4**^{sat}) and shoulders around 450 (**4**) or 420 nm (**4**^{sat}) in the visible region. UV-VIS studies on chromium complexes **5** and **5**^{sat} gave inconclusive results, presumably due to decomposition of the samples. The spectral features of **4**/**4**^{sat} indicate that each compound is capable of two different electronic transitions, with the marked blue shifts of the absorption maxima accompanying the change from an unsaturated to a saturated phosphenium unit suggesting that the NHP ligands are involved in both cases. This hypothesis was confirmed by TD-DFT calculations on model compounds **Me-4** and **Me-4**^{sat} featuring N-Me instead of the computationally prohibitively expensive N-Dipp substituents (see Figures S51 - S53 for a representation of the results). Analysis of the natural transition orbitals [36] indicates that both absorption bands can be assigned to the excitation of an electron from orbitals with pronounced 3d(Fe)/Fe-(CO,NO) bonding character into virtual orbitals that are primarily localized on the π*-orbitals of NO and NHP fragments, and exhibit accordingly strong MLCT character. As in some platinum and palladium complexes previously studied in our group,[20] the NHP ligand acts predominantly as electron accepting unit, whereas the NO ligand appears to exhibit more balanced electron donating and accepting properties.

Attempts to characterize the electron transfer behavior of the NHP/NO complexes gave only in case of **4** meaningful results. The cyclic voltammogram of a thf solution of the complex showed two reduction events at potentials of -2.33 and -2.68 V (vs. Fc/Fc^+), the first of which produced an oxidative response after reversion of the scan direction (Figure 3a). The observation that the ratio of reductive and oxidative peak currents is much smaller than unity, but increases when the scan direction is reversed immediately after the first reduction, suggests that the second electron transfer is presumably followed by a rapid chemical follow-up process whereas the first one is chemically reversible. This assumption was corroborated by IR-spectroelectrochemistry, which revealed that the three bands attributable to νCO/νNO modes of **4** were replaced upon reduction by a new pattern with a similar habitus, indicating selective formation of a new complex (Figure 3b). Prolonged electrolysis led to the appearance of additional bands attributable to unidentified follow-up products, but a recovery of up to 70% of **4** was observed upon reversal of the potential scan. An EPR spectrum recorded during electrochemical reduction contained a single broad resonance (g = 2.038, see Figure S54) which confirms the formation of an EPR-active species, but did not convey further structural information due to the lack of resolved fine structure. Based on all findings, we formulate the reduction product as a radical anion $\{\mathbf{4}\}^{\bullet-}$. The observed red shift of the νNO mode of 125 cm^{-1} upon reduction is lower than the value of 145 cm^{-1} associated with the effect of an additional unit negative charge,[11b] suggesting that the NHP ligand contributes significantly to the delocalization of the electron introduced by the reduction step. A similar conclusion has been inferred for some cobalt complexes with chelating NHP ligands.[43]

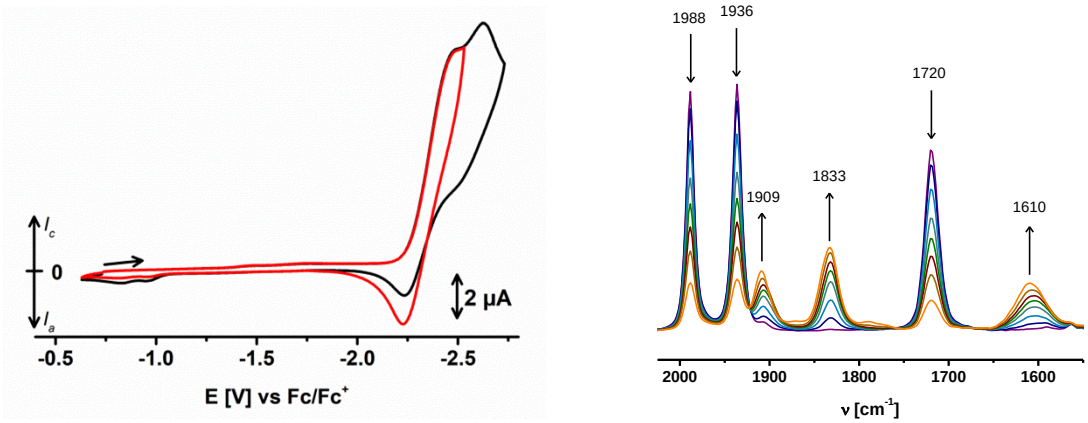

Figure 3. Representation of cyclic voltammograms (left; scan rate 15 mV/s, conducting salt Bu_4NOTf; the red trace is the result of an experiment conducted by scanning the potential over a reduced range) and an IR-spectroelectrochemistry run recorded during electrochemical reduction of a solution of **4** in thf.

Computational studies. For a further analysis of the electronic structure of NHP/NO complexes, we carried out DFT studies on N-methyl substituted model compounds **Me-4**/**Me-4**^{sat} and **Me-5**/**Me-5**^{sat} (see experimental section for details). Energy optimization of the molecular structures was performed using both B3LYP[32] and ωB97xD[33] functionals with aug-ccVDZ[34] basis sets. The solutions for **Me-4**/**Me-4**^{sat} obtained at the RωB97xD/aug-cc-pVDZ level showed RHF/UHF instability, but re-optimization using an unrestricted UωB97xD/aug-ccVDZ approach finally yielded electronically stable local minimum structures with marginally different atomic coordinates and slightly lower energies (ΔE = -0.3 (**Me-4**), -0.6 (**Me-4**^{sat}) kcal mol^{-1}). The following discussion will be based on the ωB97xD data, which give a slightly better match with the available crystallographic data of **4**/**4**^{sat} and **5**/**5**^{sat}.

The energy optimized molecular structures reproduce the P–M, M–N, and N–O distances and the effectively planar and linear coordination of the phosphorus and nitrogen donor atoms (see

Table S2), as well as the preferences of the NO ligand to occupy an equatorial site in the penta-coordinate complexes **5**/**5**^{sat} (ΔG_0 - 7.0 kcal mol^{-1} relative to the isomer with an axial NO ligand) and to avoid a perpendicular orientation of the Fe–N bond relative to the plane of the NHP ligand in **4**/**4**^{sat}. The most prominent deviation between computed and observed geometries is the tilted (in **Me-5**/**Me-5**^{sat}) vs. nearly parallel alignment (in **5**/**5**^{sat}) of the NHP ring relative to the axis of the metal coordination polyhedron. This effect has been noted before [44] and arises from the different shapes of the N-substituents in models and real complexes. A conformational search revealed that rotamers with perpendicular (in **Me-4**) or parallel (in **Me-5**) orientation of the NO ligand relative to the NPN-plane in the NHP unit are no local minima, but energetically low lying transition states ($\Delta G_0^{\neq}$ = 3.2 (**4-Me**), 5.0 (**5-Me**) kcal mol^{-1}) during rotation of the metal fragment around the M–P bond. Last, but not least, the calculated wavenumbers of νNO and νCO stretching modes for the individual local minimum structures display a close correlation with the experimental data for **4**/**4**^{sat}, **5**/**5**^{sat} and the anions $[Fe(CO)_3(NO)]^-$/$[Cr(CO)_4(NO)]^-$ (Figure S55), which led us to conclude that the computational model provides a qualitatively correct account of differential changes in the electronic structures of the compounds studied.

For a more detailed interpretation, we performed NBO [35] analyses of the computed electron densities. Even if the calculated Wiberg bond indexes (WBIs) imply, as in previously studied NHP complexes,[18,19,20,44] a substantial covalent character of the metal-ligand interactions which renders strict partitioning of electron densities between metal and ligands and a concise assignment of oxidation states disputable, inspection of atomic populations and occupancies of selected KS-orbitals or NBOs was found to allow at least a qualitative interpretation.

Natural population analyses of the chromium complexes **Me-5**/**Me-5**^{sat} predict for the NO ligands slightly negative and for the NHP ligands significantly positive partial charges (**Me-5**:

q(NO) = -0.07, q(NHP) = +0.56; **Me-5^{sat}**: q(NO) = -0.06, q(NHP) = 0.63). Analysis of the NBOs suggests that the atoms in the NO unit are connected by a double bond, and that both the NHP and NO ligands interact with the metal atom through a combination of dative N→Cr or P→Cr σ-bonds and covalent π-bonds. These interactions are associated with net shifts of electron density from the NO ligand to the metal carbonyl fragment, and from the metal carbonyl fragment to the NHP moiety. As the second effect is less pronounced, we note a build-up of an excess negative charge on the $Cr(CO)_3$ fragment and an increased population of the metal d-orbitals ($d^{6.38/6.36}$ for **Me-5**/**Me-5^{sat}** vs. d^6 for a chromium atom in formal oxidation state zero), while the NHP unit retains a positive partial charge and is expected to maintain electrophilic character (which is in line with the assignment of the electronic transitions, vide supra). In total, the metal-ligand bonding may be depicted in terms of a neutral $Cr(CO)_3$ unit interacting with an anionic σ-/π-donor nitroxide (NO^-) and a cationic σ-donor/π-acceptor NHP ligand. The minor difference in NHP partial charges for **Me-5^{sat}**/**5-Me** (q(NHP) = 0.56/0.63) suggests, in line with the IR data, that the saturated NHP is a slightly better π-acceptor. We note, however, that the observation of a 3-center-4-electron interaction which reinforces the Cr–N bond (cf. WBI(Cr–N) = 1.29/1.30 vs. WBI(Cr–P) = 0.82/0.87 for **Me-5**/**Me-5^{sat}**) and weakens the N–O bond (WBI(N–O) = 1.77 for **Me-5**, **Me-5^{sat}**) and the partial population of antibonding π*(Cr–N) and π*(Cr–P) NBOs give a strong indication that the electron structure is strongly delocalized, and a correct description requires presumably the consideration of several resonance structures.

The natural population analyses of the UωB97xD/aug-ccVDZ densities of the iron complexes **Me-4**/**Me-4^{sat}** suggest a stronger flow of electron charge towards the NO ligand, while the charge state of the NHP ligands is similar as in the chromium complexes (**Me-4**: q(NO) = -0.26, q(NHP) = +0.60; **Me-4^{sat}**: q(NO) = -0.24, q(NHP) = 0.54). The negative partial charges on the $Fe(CO)_2$

fragment (-0.34/-0.30 for **Me-4**/**Me-4^{sat}**) and metal d-electron populations ($d^{7.81}$ in both species) indicate that the metal oxidation state (possibly averaged over different resonance structures [14]) remains close to zero. In line with a smaller deviation of the actual charge distribution from the 'idealized' situation $NHP^{+}/Fe(CO)_2^{0}/NO^{-}$ than in the chromium complexes, the WBIs characterizing the covalent P–Fe (0.71/0.75 for **Me-4**/**Me-4^{sat}**) and Fe–N (1.06/1.06 for **Me-4**/**Me-4^{sat}**) bonding contributions are lower than in **Me-5**/**Me-5^{sat}**, whereas the NO-bond (WBI 1.79 for both compounds) remains essentially unaffected. Further interpretation of NBOs is difficult, as the bonding in α- and β-spin manifolds differs substantially. However, some insight is gained from inspection of the spin density, which discloses significant excess populations of α- and β-spins residing in the π-electron system of the NO ligand (n_α = 0.73/0.67 for **Me-4**/**Me-4^{sat}**) and iron d-orbitals (n_β = 0.78/0.71 for **Me-4**/**Me-4^{sat}**), respectively (Figure 4).

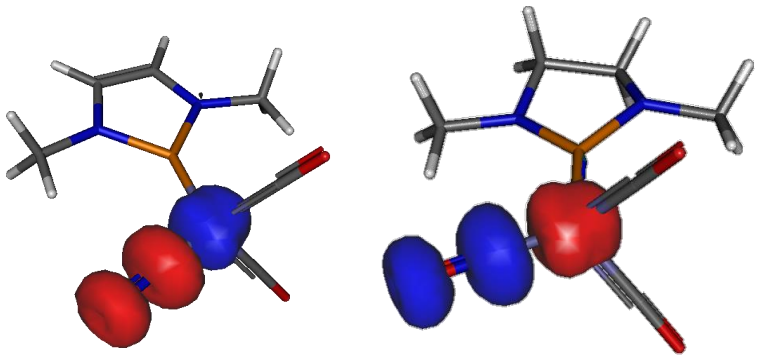

Figure 4. Graphical representation of the spin density distribution for the iron complexes **Me-4** (left) and **Me-4^{sat}** (right) calculated at the UωB97xD/aug-ccVDZ level of theory. Blue and red isosurfaces denote α- and β-spin density.

The observed spin density distribution implies that a depiction of the bonding in **Me-4**/**Me-4^{sat}** cannot be given in terms of a single electron configuration, but requires as in case of the Hieber anion $[Fe(CO)_3(NO)]^{-}$ [14] a multi-configurational approach. This hypothesis is backed by a

CASPT2(4,4) calculation on a model compound **H-4** (with N-H instead of N-Me substituents), which was performed at the DFT-optimized molecular geometry using two metal d-orbitals and the π*(NO) orbitals as the active space. Inspection of the resulting wave function (Table S3) allowed us to identify the leading electron configuration as antiferromagnetically coupled combination of $^{3}\{(NHP)Fe(CO)_2\}^{+}$ and $^{3}\{NO\}^{-}$ fragments (34 %), with further contributions from configurations composed of $^{1}\{(NHP)Fe(CO)_2\}^{+}$/ $^{1}\{NO\}^{-}$ (36 %) and antiferromagnetically coupled $^{2}\{(NHP)Fe(CO)_2\}^{\bullet/2}\{NO\}^{\bullet}$ (18 %) and $^{2}\{(NHP)Fe(CO)_2\}^{2+/2}\{NO\}^{2-}$ (12 %) fragments, respectively. This bonding description compares qualitatively with the situation established for $[Fe(CO)_3(NO)]^{-}$,[14] even if formal replacement of one CO by a positively charged NHP reduces the anionic character of the NO ligand and strengthens the P–M π-bonding.

In order to validate the identity of the species formed by reduction of **4** (vide supra), we also carried out calculations on the model radical anion $\{\mathbf{Me\text{-}4}\}^{\bullet-}$. Energy optimization at the UωB97xD/aug-ccVDZ level converged to a doublet state with a molecular geometry characterized by quasilinear MNO (Fe–N–O 175.9°) and pyramidal NHP moieties (sum of bond angles at P 322.3°; Figure 5). The Fe–P (2.187 Å), Fe–N (1.693 Å) and N–O distances (1.203 Å) are longer than in **Me-4** (Fe–P/Fe–N/N–O 2.035/1.654/1.174 Å). The calculated wavenumbers for νNO and νCO modes of $\{\mathbf{Me\text{-}4}\}^{\bullet-}$ obey the correlation between calculated and experimental data observed for the remaining (model) compounds in this study (Figure S55), which we interpret as corroboration of the correctness of our proposed assignment of the reduction product.

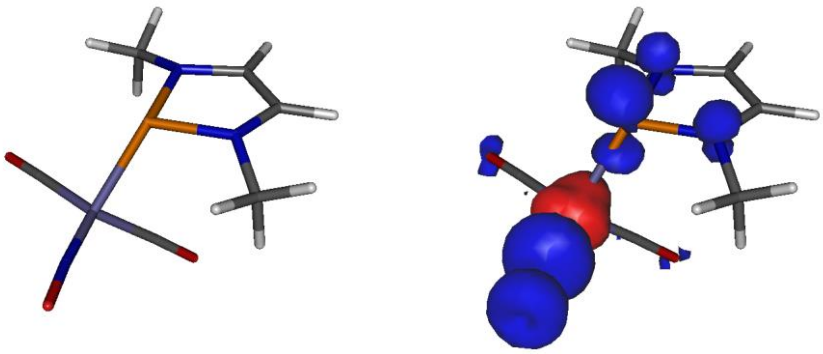

Figure 5. Graphical representation of the energy optimized molecular structure (left) and spin density (right; blue and red isosurfaces denote α- and β-spin density) for {**Me-4**}$^{\bullet-}$ calculated at the UωB97xD/aug-ccVDZ level of theory.

A natural population analysis indicates that half of the extra charge conveyed to {**Me-4**}$^{\bullet-}$ during reduction is attracted by the NHP unit (q(NHP) = +0.05; Δq = -0.49 compared to **Me-4**), whereas the remaining excess electron density is nearly evenly distributed over the Fe(CO)$_2$ (q = -0.56; Δq = -0.22) and NO units (q = -0.49, Δq = -0.23). The metal d-electron population ($d^{7.72}$ vs. $d^{7.81}$ in **Me-4**) remains unaffected. The calculated spin density of {**Me-4**}$^{\bullet-}$ (Figure 5) features excess populations of α- and β-spins in the NO (n_α = 1.13) and Fe(CO)$_2$ regions (n_β = 0.84), which are similar to those computed for **Me-4**, along with additional α-spin density (n_α = 0.71) residing in a π*-orbital centered on the NPN region of the NHP ligand. In accord with this finding, we note that the leading contributions to the CASPT2(5,5)/cc-pVDZ wave function of the parent radical anion {**H-4**}$^{\bullet-}$ arise from configurations that can be obtained by merging the combinations of ^{3}{Fe(CO)$_2$}/^{3}{NO}$^-$, ^{1}{Fe(CO)$_2$}/^{1}{NO}$^-$ and ^{2}{Fe(CO)$_2$}$^-$/^{2}{NO} fragments established for neutral **H-4** with an additional ^{2}{NHP•} fragment to a state with S = ½ (see Table S4). The high radical character of the metal-bound NHP fragment implied by the DFT and CASPT2 calculations is consistent with previous findings on complexes [(Ph$_2$P•)M(CO)$_5$] (M = Cr, Mo, W).[45] Moreover, comparing the computed charge and spin density distributions for **Me/H-4** and {**Me/H-4**}$^{\bullet-}$

supports the depiction of the reduction as a predominantly (although not entirely) phosphenium centered event, which implies close parallels to the behavior of previously reported cobalt NHP complexes [43] and further manifests the proposed [8] non-innocence of metal-bound NHP ligands.

Reactivity Studies. The assessment of donor properties and "philicity" of the NHP and NO ligands in **4**/**4**^{sat} and **5**/**5**^{sat} is not only feasible from spectroscopic or computational data, but also from a study of the chemical behavior of the complexes towards nucleophiles or electrophiles. For instance, our group has recently used the transfer of hydride or a methyl anions to the phosphorus atom of manganese complex **VI** (Scheme 1) to illustrate the electrophilic behavior of the metal-bound NHP ligand,[18] whereas Thomas et al. [21] demonstrated that a (nucleophilic) phosphide-type NHP-unit in a cobalt complex failed to react with hydride sources. Moreover, Douglas and Feltham used a reaction with azide ion to assign the charge state of a NO ligand.[46] The observed addition under formation of a five-membered heterocycle which immediately decomposed under release of N_2 and N_2O can only take place when the ligand has nitrosonium (NO^+), and thus electrophilic, character.

Reactions of **4**/**4**^{sat} or **5**/**5**^{sat} with an equimolar amount of superhydride ($LiBEt_3H$) proceeded under selective hydride transfer to afford complexes Li[**6**]/Li[**6**^{sat}] and Li[**7**]/Li[**7**^{sat}] (Scheme 3), respectively. All products were unequivocally identified by NMR data, and a salt PPh_4[**6**] was isolated after cation exchange and fully characterized. The presence of a secondary phosphine ligand in each species is evidenced by the characteristic doublet splitting of the ^{31}P NMR signal ($^1J_{PH}$ = 286 – 301 Hz) and the large positive chemical shift of the P-bound hydrogen atom (δ^1H 9.83 to 9.76 ppm) ranging far outside the negative shift region expected for metal hydrides.

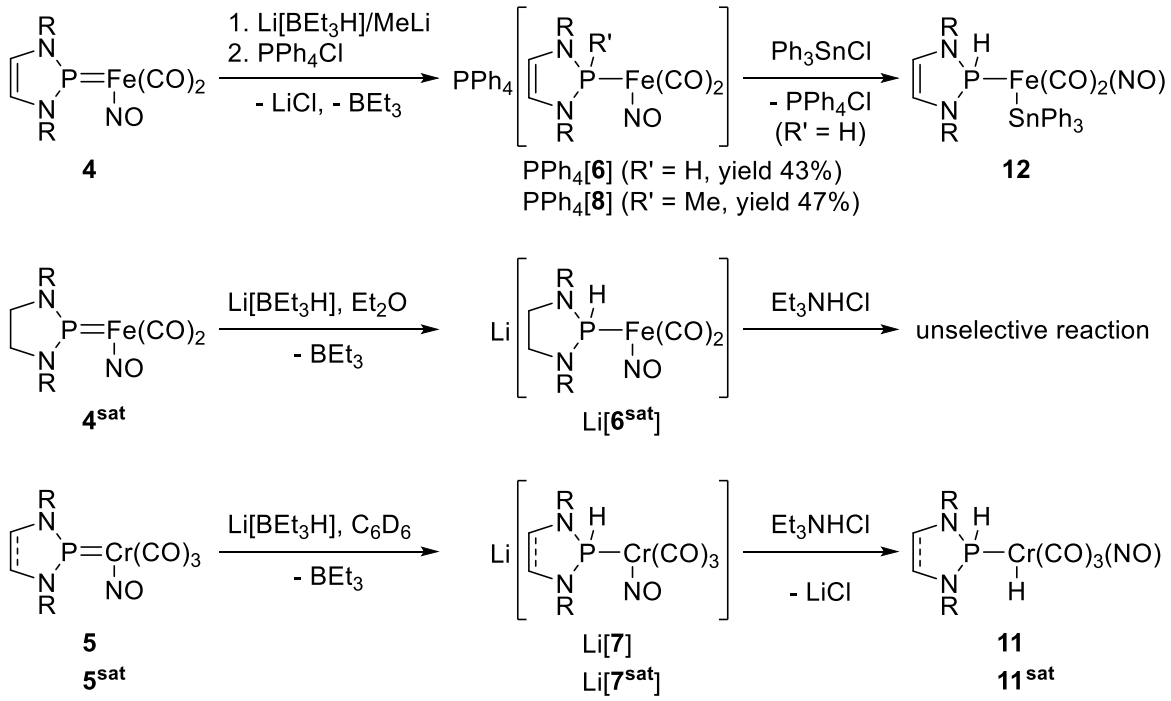

Scheme 3. Reactions associated with treatment of complexes **4**, **4**^{sat}, **5**, **5**^{sat} with super hydride and methyl lithium, respectively (R = 2,6-*i*Pr$_2$C$_6$H$_3$ (Dipp)).

The constitution of PPh$_4$[**6**] was confirmed by a single-crystal x-ray diffraction study (Figure 6). The coordination at both iron and the phosphorus atoms (where the attached hydrogen atom H1 was localized and refined freely) is distorted tetrahedral. The NO ligand is not disordered, but occupies a specific site characterized by a transoid alignment of the N–Fe–P–H array. The P–Fe bond (2.1339(9) Å) is intermediate between the values observed for **4**/**4**^{sat} (2.0291(6) – 2.0331(5) Å) and iron carbonyl complexes of secondary phosphines (2.140 – 2.417 Å[47]), indicating that π-back-bonding is weaker than in the NHP complexes but still operative.

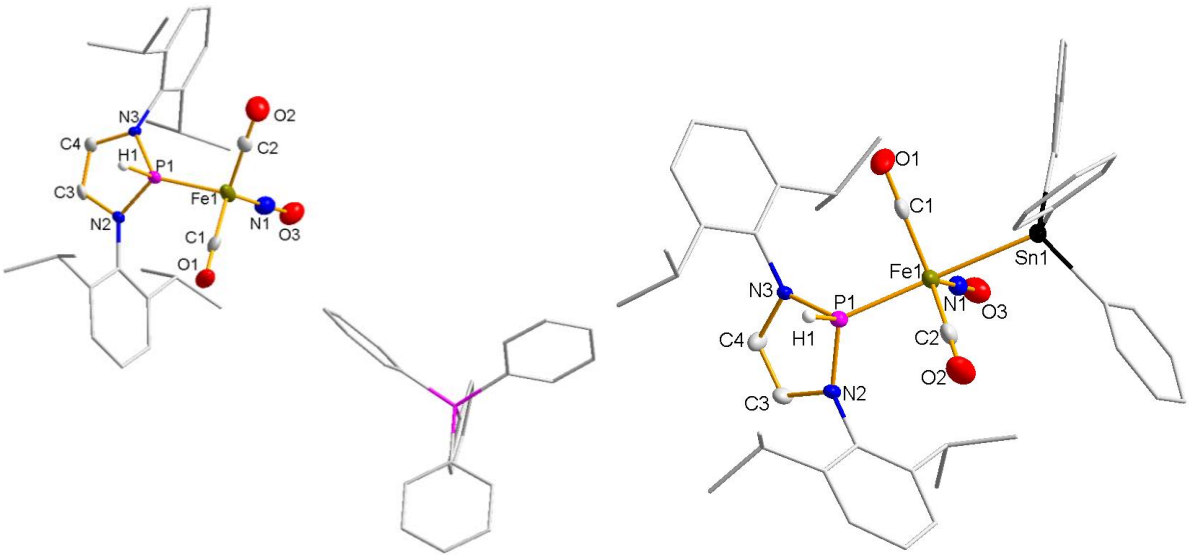

Figure 6 View of the molecular structures of PPh_4[**6**] (left) and **12** (right). For clarity, C–H hydrogen atoms and a solvent molecule (toluene) were omitted, and peripheral substituents as well as the cation of PPh_4[**6**] represented using a wire model. Thermal ellipsoids are drawn at the 50 % probability level. Selected distances [Å] and angles [°] are listed in Table 2.

A similar behavior as towards hydride was also established for the reaction of **4** with methyl lithium to yield an anionic diazaphospholene complex **8**$^-$, which was likewise isolated as a tetraphenylphosphonium salt (Scheme 3). The constitution of PPh_4[**8**] was established from analytical and spectral data and qualitatively confirmed by a single-crystal XRD study (see Figure S1; even if the structure could be solved, low crystal quality impeded its satisfactory refinement, and we refrain from a more detailed discussion).

Reaction of **4** with sodium azide afforded as the main phosphorus-containing species 2-azido diazaphospholene **9**[27] and secondary diazaphospholene oxide **10**[28] (arising from hydrolysis by adventitious water), both of which were identified in the reaction mixture by comparing the observed NMR data with those of authentic samples (Scheme 4). Even if the fate of the metal

fragment remains unknown, we assume that product formation is initiated, as in the reactions with super hydride and methyl lithium, by a nucleophilic attack on the NHP ligand.

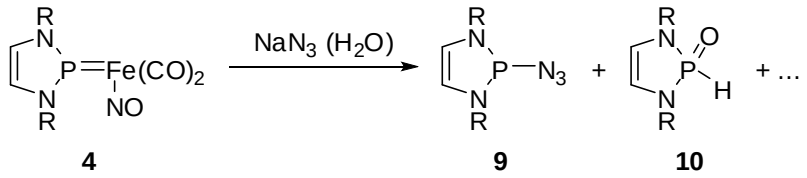

4 **9** **10**

Scheme 4. Reaction of complex **4** with sodium azide (R = 2,6-*i*Pr$_2$C$_6$H$_3$ (Dipp)).

As in case of **VI**,[18a] we further explored the possibility to protonate anions [**6**]$^-$/[**6**^{sat}]$^-$ and [**7**]$^-$ /[**7**^{sat}]$^-$ to afford neutral species that can be regarded as formal hydrogenation products of the original NHP complexes. Treatment of Li[**6**] or PPh$_4$[**6**] with Et$_3$NHCl, which had been successfully employed in the analogous reaction of **VI**,[18] or acetic acid resulted in re-formation of **4**, while reaction of PPh$_4$[**6**] with the stronger acid H(OEt$_2$)$_2$[TRISPHAT] [25] was unselective and afforded a mixture of **4** with further unidentified phosphorus-containing species. An erratic transformation with partial regeneration of phosphenium complex **4**^{sat} was also observed between Li[**6**^{sat}] and Et$_3$NHCl. Trapping of the anion of PPh$_4$[**6**] with methyl iodide and Me$_3$SiCl failed, but reaction with Ph$_3$SnCl proceeded smoothly to afford neutral complex **12** (Scheme 3), which was readily isolated and fully characterized. Crystalline **12** (Figure 6) contains complexes built around a tbp-coordinated iron center with axial Ph$_3$Sn and secondary phosphine, and equatorial CO and NO units. The conformational orientation at the central Fe–P bond with a transoid N–Fe–P–H array is similar as in PPh$_4$[**6**], but the additional lengthening of the Fe–P bond (2.1755(12) Å) suggests that the electrophilic stannyl ligand reduces the M→P π-back-donating capability of the metal fragment even further. This is also in accord with the blue shift of the νCO and νNO stretching modes of **12** by about 100 cm^{-1} compared to PPh$_4$[**6**].

Chromium complexes Li[**7**]/Li[**7**^{sat}] were found to undergo clean protonation with Et_3NHCl to secondary phosphine metal hydrides **11** and **11**^{sat} (Scheme 3), which could not be isolated in pure form but were identified spectroscopically. Key to the structural assignment is the observation of ^{1}H NMR signals for the mutually coupled metal-bound (**11**: δ -5.40 ppm, dd, $^2J_{PH}$ = 55 Hz, $^3J_{HH}$ = 2.2 Hz; **11**^{sat} δ -5.23 ppm, dd, $^2J_{PH}$ = 52 Hz, $^3J_{HH}$ = 1.9 Hz) and phosphorus-bound (**11**: δ 8.84, dd, $^1J_{PH}$ = 312 Hz, $^3J_{HH}$ = 2.2 Hz; **11**^{sat} δ 8.27 ppm, br d, $^1J_{PH}$ = 310 Hz) hydrogen atoms.

Conclusions

Carbonyl complexes of chromium and iron featuring both N-heterocyclic phosphenium (NHP) and nitrosyl (NO) ligands were synthesized by metathesis between ionic NHP triflates and metallates PPN[M(CO)$_n$(NO)]. Structural, spectroscopic and computational studies suggest describing the NHP fragments as formally cationic carbene-analogue ligands with weak σ-donor and pronounced π-acceptor character, and the NO moieties as formally anionic nitroxide (NO^-) units. Accordingly, the two types of ligands are not rivaling π-acceptors which compete in withdrawing electron density from the metal center, but cooperate in creating a "push-pull" situation that levels the ligand charge states via π-type interactions. Obviously, the electronegative nitrogen atom provides for the best stabilization of excess negative charge, and the shifts in electron density associated with the π-interactions are too small to equalize or even overturn the initial charge gradient expressed in the formal charge states +1(NHP)/0(M)/-1(NO). The computational results suggest that the electronic structure of iron complexes [(NHP)Fe(CO)$_2$(NO)] compares closely with that of the Hieber anion $[Fe(CO)_3(NO)]^-$,[14] thus further emphasizing the perception of NHP ligands as isoelectronic analogues of CO with increased π-acceptor ability, and imply that the preference of the NO ligand to adopt an anionic charge state may be of wider importance in the chemistry of low valent transition metal complexes. The electrophilic nature of

the metal-bound NHP ligands is further confirmed by the chemical behavior of the complexes. Reactions with super hydride or methyl lithium afford anionic phosphine complexes that are trappable by electrophiles and make interesting candidates for nucleophilic catalysts.[48] The reaction of [(NHP)Fe(CO)$_2$(NO)] with azide ion to yield an azido-phosphine corroborates both the electrophilic properties of the NHP unit and the absence of a notable electrophilic character of the nitroxide ligand. Electrochemical reduction of this complex produced a transient radical anion [(NHP)Fe(CO)$_2$(NO)]$^{\bullet-}$. Comparison of observed and computed IR data as well as computed spin density distributions for the neutral precursor and the radical anion suggest that the reduction is mainly, but not entirely, phosphenium centered, which implies close parallels to the previously reported behavior of some cobalt NHP complexes [43] and further manifests the proposed [8] non-innocence of metal-bound NHP ligands. Further elaboration of the reductive approach may open an avenue for accessing further examples of elusive complexes [45] with P-centered radical ligands.

ASSOCIATED CONTENT

Supporting Information. The following files are available free of charge.

Details on the crystal structure determinations of **4**, **4^{sat}**, **5**, **5^{sat}**, PPh$_4$[**6**], PPh$_4$[**8**] and **12**; molecular structure of PPh$_4$[**8**], NMR and IR spectra of **4**, **4^{sat}**, **5**, **5^{sat}**, PPh$_4$[**6**], PPh$_4$[**8**], **11** and **12**; UV-VIS spectra of **4** and **4^{sat}**; cyclic voltammetry and IR-SEC studies of the reduction of **4**; NMR spectra of the reactivity studies; results of DFT and CASPT2 calculations, full citation of ref. 31 (PDF).

Crystal structure data for **4**, **4^{sat}**, **5**, **5^{sat}**, PPh$_4$[**6**], PPh$_4$[**8**] and **12** (CIF).

AUTHOR INFORMATION

Corresponding Author

* E-mail: gudat@iac.uni-stuttgart.de.

Author Contributions

The manuscript was written through contributions of all authors. All authors have given approval to the final version of the manuscript.

Funding Sources

INST 40/467-1 FUGG (JUSTUS cluster)

ACKNOWLEDGMENT

The authors thank the Institut für Anorganische Chemie for financial support. We further thank B. Förtsch for elemental analyses and Dr. W. Frey (Institut für Organische Chemie) for collecting the x-ray data sets. The computational studies were supported by the state of Baden-Württemberg through bwHPC and the German Research Foundation (DFG) through grant no INST 40/467-1 FUGG (JUSTUS cluster).

ABBREVIATIONS

Dipp, 2,6-diisopropyl-phenyl; NHP, N-heterocyclic phosphenium ion; PPN, nitride-bis-triphenylphosphonium cation; TRISPHAT, tris-(tetrachloro-benzenediolato)phosphate.

REFERENCES

1 Light, R. W.; Paine, R. T. Interaction of the Dicoordinate Phosphorus Cation 1,3-Dimethyl-1,3,2-Diazaphospholidide with Transition Metal Nucleophiles. *J. Am. Chem. Soc*. **1978**, *100*, 2230–2231.

2 Montemayor, R. G.; Sauer, D. T.; Fleming, S.; Bennett, D. W.; Thomas, M. G.; Parry, R.

W. Iron Carbonyl Complexes Containing Positively Charged Phosphorus Ligands. *J. Am. Chem. Soc*. **1978**, *100*, 2231–2233.

3 Reviews: (a) Cowley, A. H.; Kemp, R. A. Synthesis and Reaction Chemistry of Stable Two-Coordinate Phosphorus Cations (Phosphenium Ions). *Chem. Rev*. **1985**, *85*, 367–382; (b) Sanchez, M.; Mazières, R. M.; Lamandé, L.; Wolf R. Phosphenium Cations. In *Multiple Bonds and Low Coordination in Phosphorus Chemistry*; Regitz, M., Scherer, O. J., Eds.; Thieme: Stuttgart, **1990**; pp 129–156; (c) Gudat, D. Cationic Low Coordinated Phosphorus Compounds as Ligands: Some Recent Developments. *Coord. Chem. Rev*. **1997**, *173*, 71–106; (d) Nakazawa, H. Transition Metal Complexes Bearing a Phosphenium Ligand. *Adv. Organomet. Chem*. **2004**, *50*, 108–143; (e) Rosenberg, L. Metal Complexes of Planar PR_2 Ligands: Examining the Carbene Analogy. *Coord. Chem. Rev*. **2012**, *256*, 606–626; (f) Gudat, D. Low-Coordinate Main Group Compounds - Group 15. In *Compreh. Inorg. Chem. II*; Reedijk, J.; Poeppelmeier, K., Ed.; Elsevier: Oxford **2013**, Vol 1, pp 587–621.

4 Hutchins, L. D.; Duesler, E. N.; Paine, R. T. Structure and Bonding in a Phosphenium Ion-Iron Complex, $Fe[\eta^5\text{-}(CH_3)_5C_5](CO)_2[PN(CH_3)CH_2CH_2NCH_3]$. A Demonstration of Phosphenium Ion Acceptor Properties. *Organometallics* **1982**, *1*, 1254 –1256.

5 Pan, B. Bezpalko, M. W. Foxman, B. M. Thomas, C. M. Coordination of an N-Heterocyclic Phosphenium Containing Pincer Ligand to a $Co(CO)_2$ Fragment Allows Oxidation To Form an Unusual N-Heterocyclic Phosphinito Species. *Organometallics* **2011**, *30*, 5560−5563.

6 Green, M. L. H. A New Approach to the Formal Classification of Covalent Compounds of the Elements. *J. Organomet. Chem*. **1995**, *500*, 127–148.

7 Burck, S.; Daniels, J.; Gans-Eichler, T.; Gudat, D.; Nättinen, K.; Nieger, M. *N*-Heterocyclic Phosphenium, Arsenium, and Stibenium Ions as Ligands in Transition Metal Complexes: A Comparative Experimental and Computational Study. *Z. Anorg. Allg. Chem*. **2005**, *631*, 1403–1412.

8 Pan, B.; Xu, Z.; Bezpalko, M. W.; Foxman, B. M.; Thomas, C. M. N-Heterocyclic Phosphenium Ligands as Sterically and Electronically-Tunable Isolobal Analogues of Nitrosyls. *Inorg. Chem*. **2012**, *51*, 4170–4179.

9 Review: Kaim, W.; Schwederski, B. Non-Innocent Ligands in Bioinorganic Chemistry - An Overview. *Coord. Chem. Rev*. **2010**, *254*, 1580–1588.

10 Jørgensen, C. K. Differences between the Four Halide Ligands, and Discussion Remarks on Trigonal-Bipyramidal Complexes, on Oxidation States, and on Diagonal Elements of One-Electron Energy. *Coord. Chem. Rev*. **1966**, *1*, 164–178.

11 Selected Reviews: (a) Roncaroli, F.; Videla, M.; Slep, L. D.; Olabe, J. A. New features in the redox coordination chemistry of metal nitrosyls {M–NO^+; M–NO•; M–NO^-(HNO)}. *Coord. Chem. Rev*. **2007**, *251*, 1903–1930; (b) de la Cruz, C.; Sheppard, N. A structure-based analysis of the vibrational spectra of nitrosyl ligands in transition-metal coordination complexes and clusters. *Spectrochim. Acta A* **2011**, *78*, 7–28; (c) Lewandowska, H. Spectroscopic Characterization of Nitrosyl Complexes. *Struct. Bond*. **2014**, *153*, 115–165.

12 Enemark, J. H.; Feltham, R. D. Principles of Structure, Bonding, and Reactivity for Metal Nitrosyl Complexes. *Coord. Chem. Rev*. **1974**, *13*, 339–406.

13 (a) Cheng, H.-Y.; Chang, S.; Tsai, P.-Y. On the "brown-ring" reaction product via density-

functional theory. *J. Phys. Chem. A* **2004**, 108, 358–361; (b) Wanat, A.; Schneppensieper, T.; Stochel, G.; van Eldik, R.; Bill, E.; Wieghardt, K. Kinetics, Mechanism, and Spectroscopy of the Reversible Binding of Nitric Oxide to Aquated Iron(II). An Undergraduate Text Book Reaction Revisited. *Inorg. Chem*. **2002**, *41*, 4–10.

14 Klein, J. E. M. N.; Miehlich, B.; Holzwarth, M. S.; Bauer, M.; Milek, M.; Khusniyarov, M. M.; Knizia, G.; Werner, H.-J.; Plietker, B. The Electronic Ground State of $[Fe(CO)_3(NO)]^-$: A Spectroscopic and Theoretical Study. *Angew. Chem. Int. Ed*. **2014**, *53*, 1790–1794.

15 McCleverty J. A. Chemistry of Nitric Oxide Relevant to Biology. *Chem. Rev*. **2004**, *104*, 403–418.

16 A high degree of covalency in the metal-ligand bond may also frustrate a simple interpretation of the bonding situation in NHP complexes, see: Nickolaus, J.; Imbrich, D. A.; Schlindwein, S. H.; Geyer, A. H.; Nieger, M.; Gudat, D. Phosphenium Hydride Reduction of $[(Cod)MX_2]$ (M = Pd, Pt; X = Cl, Br): Snapshots on the Way to Phosphenium Metal(0) Halides and Synthesis of Metal Nanoparticles. *Inorg. Chem*. **2017**, *56*, 3071–3080.

17 Pan, B.; Bezpalko, M. W.; Foxman B. M.; Thomas, C. M. Heterolytic addition of E–H bonds across Pt–P bonds in Pt N-heterocyclic phosphenium/phosphido complexes. *Dalton Trans*. **2012**, *41*, 9083–9090.

18 (a) Gediga, M.; Feil, C. M.; Schlindwein, S. H.; Bender, J.; Nieger, M.; Gudat, D. N-Heterocyclic Phosphenium Complex of Manganese: Synthesis and Catalytic Activity in Ammonia Borane Dehydrogenation. *Chem. – Eur. J*. **2017**, *23*, 11560–11569; (b) Gediga, M.; Schlindwein, S. H.; Bender, J.; Nieger, M.; Gudat, D. Variable Reactivity of a N-Heterocyclic Phosphenium

Complex: P−C Bond Activation or “Abnormal” Deprotonation. *Angew. Chem. Int. Ed*. **2017**, *56*, 15718–15722.

19 Stadelmann, B.; Bender, J.; Förster, D.; Frey, W.; Nieger, M.; Gudat, D. An Anionic Phosphenium Complex as an Ambident Nucleophile. *Dalton Trans*. **2015**, *44*, 6023–6031.

20 For NHP ions, see: Förster, D.; Nickolaus, J.; Nieger, M.; Benkő, Z.; Ehlers, A. W.; Gudat, D. Donor-Free Phosphenium−Metal(0)−Halides with Unsymmetrically Bridging Phosphenium Ligands. *Inorg. Chem*. **2013**, *52*, 7699−7708.

21 Poitras, A. M.; Knight, S. E.; Bezpalko, M. W.; Foxman, B. M.; Thomas, Christine M. Addition of H_2 Across a Cobalt–Phosphorus Bond. *Angew. Chem. Int. Ed*. **2018**, *57*, 1497–1500.

22 Burck, S.; Gudat, D.; Nättinen, K.; Nieger, M.; Niemeyer, M.; Schmid, D. 2-Chloro-1,3,2-Diazaphospholenes – A Crystal Structural Study. *Eur. J. Inorg. Chem*. **2007**, 5112–5119.

23 Stevens, R. E.; Gladfelter, W. L. Nucleophilic Nitrosylations of Metal Carbonyls Using Bis(Triphenylphosphine)Nitrogen(1+) Nitrite. *Inorg. Chem*. **1983**, *22*, 2034–2042.

24 Mantell, D. R.; Gladfelter, W. L. Synthesis, Characterization, and Reactivity of PPN[$Cr(CO)_4(NO)$]. *J. Organomet. Chem*. **1988**, *347*, 333–342.

25 Siu, P. W.; Hazin, K.; Gates, D. P. $H(OEt_2)_2[P(1,2\text{-}O_2C_6Cl_4)_3]$: Synthesis, Characterization, and Application as a Single-Component Initiator for the Carbocationic Polymerization of Olefins. *Chem. Eur. J*. **2013**, *19*, 9005–9014.

26 Abrams, M. B.; Scott, B. L.; Baker, R. T. Sterically Tunable Phosphenium Cations: Synthesis and Characterization of Bis(Arylamino)Phosphenium Ions, Phosphinophosphenium

Adducts, and the First Well-Defined Rhodium Phosphenium Complexes. *Organometallics* **2000**, *19*, 4944–4956.

27 Gediga, M.; Burck, S.; Bender, J.; Förster, D.; Nieger, M.; Gudat, D. Specific and Reversible Alkynyl Transfer Reactions of an N-Heterocyclic Phosphane. *Eur. J. Inorg. Chem*. **2014**, 1818–1825.

28 Li, Z.; Chen, X.; Bergeler, M.; Reiher, M.; Su, C.-Y.; Grützmacher, H. A stable phosphanyl phosphaketene and its reactivity. *Dalton Trans*. **2015**, *44*, 6431–6438.

29 Sheldrick, G. M. A Short History of SHELX. *Acta Crystallogr. A* **2008**, *64*, 112–122.

30 Krejčik, M.; Daněk, M.; Hartl, F. Simple Construction of an Infrared Optically Transparent Thin-Layer Electrochemical Cell. *J. Electroanal. Chem. Interfacial Electrochem.* **1991**, *317*, 179–187.

31 G. M. J. Frisch et al., Gaussian 09, Revision D.01, Gaussian, Inc.: Wallingford, CT, 2009.

32 Becke, A. D. Density-functional thermochemistry. III. The role of exact exchange. *J. Chem. Phys*. **1993**, *98*, 5648–5652.

33 Chai, J.-D.; Head-Gordon, M. Long-range corrected hybrid density functionals with damped atom-atom dispersion corrections, *Phys. Chem. Chem. Phys.* **2008**, *10*, 6615–6620.

34 (a) Dunning Jr., T. H. Gaussian basis sets for use in correlated molecular calculations. I. The atoms boron through neon and hydrogen, *J. Chem. Phys.* **1989**, *90*, 1007–1023; (b) Woon, D. E.; Dunning Jr., T. H. Gaussian-basis sets for use in correlated molecular calculations. 3. The atoms aluminum through argon, *J. Chem. Phys.* **1993**, *98*, 1358–71; (c) Balabanov, N. B.; Peterson,

K. A. Systematically convergent basis sets for transition metals. I. All-electron correlation consistent basis sets for the elements Sc–Zn. *J. Chem. Phys*. **2005**, *123*, 064107.

35 Glendening, E. D.; Badenhoop, J. K.; Reed, A. E.; Carpenter, J. E.; Bohmann, J. A.; Morales, C. M.; Landis, C. R.; Weinhold, F. NBO 6.0. Theoretical Chemistry Institute, University of Wisconsin, Madison, **2013**.

36 Martin, R. L. Natural transition orbitals. *J. Chem. Phys.* **2003**, *118*, 4775–4777.

37 Allouche, A. R. Gabedit – a graphical user interface for computational chemistry softwares. *J. Comput. Chem*. 2011, **32**, 174–182.

38 Nakazawa, H.; Yamaguchi, Y.; Mizuta, T.; Miyoshi, K. Cationic Phosphenium Complexes of Group 6 Transition Metals: Reactivity, Isomerization, and X-Ray Structures. *Organometallics* **1995**, *14*, 4173–4182.

39 Pannell, K. H.; Chen, Y. S.; Belknap, K.; Wu, C. C.; Bernal, I.; Creswick, M. W.; Huang, H. N. Structure and Reactivity of $M^+[Fe(CO)_3(NO)]^-$. *Inorg. Chem*. **1983**, *22*, 418–427.

40 Cowley, A. H.; Kemp, R. A.; Ebsworth, E. A. V.; Rankin, D. W. H.; Walkinshaw, M. D. Structure/Reactivity Relationships for Cationic (Phosphenium)Iron Tetracarbonyl Complexes. *J. Organomet. Chem*. **1984**, *265*, C19–C21.

41 Clarkson, L. M.; Clegg, W.; Hockless, D. C. R.; Norman, N. C. Structure of a Thallium(I) Transition-Metal Carbonyl Salt $Tl[Fe(CO)_3(NO)]$. *Acta Crystallogr. Sect. C* **1992**, *48*, 236–239.

42 Gudat, D.; Haghverdi, A.; Nieger, M. Complexes with phosphorus analogues of imidazoyl carbenes: unprecedented formation of phosphenium complexes by coordination induced P–Cl

bond heterolysis. *J. Organomet. Chem*. **2001**, *617–618*, 383–394.

43 Bezpalko, M. W.; Poitras, A. M.; Foxman, B. M.; Thomas Christine M. Cobalt N-Heterocyclic Phosphenium Complexes Stabilized by a Chelating Framework: Synthesis and Redox Properties. *Inorg. Chem*. **2017**, *56*, 503−510.

44 Papendick, M.; Feil, C. M.; Nieger, M.; Gudat, D. Steric control in reactions of N-heterocyclic phosphorus electrophiles with pentacarbonyl manganate(-I). *Z. Anorg. Allg. Chem.* **2018**, *644*, 1006–1010.

45 Ndiaye, B.; Bhat, S.; Jouaiti, A.; Berclaz, T.; Bernardinelli, G.; Geoffroy M. EPR and DFT Studies of the Structure of Phosphinyl Radicals Complexed by a Pentacarbonyl Transition Metal. *J. Phys. Chem. A* **2006**, *110*, 9736–9742.

46 Douglas, P. G.; Feltham, R. D. Reactions of Coordinated Ligands. II. Azide and Dinitrogen Complexes of Ruthenium. *J. Am. Chem. Soc*. **1972**, *94*, 5254–5258.

47 Determined by a query in the CSD data base for secondary phosphine carbonyl iron complexes (29.06.18, 79 entries).

48 Plietker, B. A highly regioselective salt-free iron-catalyzed allylic alkylation. *Angew. Chem. Int. Ed*. **2006**, *45*, 1469–1473.

SYNOPSIS Mixed complexes [(NHP)M(CO)$_n$(NO)] (M = Fe, Cr; n = 2, 3) containing both N-heterocyclic phosphenium (NHP) and nitrosyl (NO) ligands were synthesized and characterized by structural, spectroscopic and computational studies. The two types of ligands behave as complementary σ-donor/π-acceptor (NHP$^+$) and σ-donor/π-donor (NO$^-$) moieties. The NHP$^+$ unit displays non-innocent behavior during reduction and acts as electrophilic center in chemical reactions with nucleophiles.